

Quantum Phase Transitions

G. G. Batrouni

*INLN, Université de Nice-Sophia Antipolis, CNRS; 1361 route des Lucioles, 06560 Valbonne,
France*

R. T. Scalettar

Physics Department, University of California, Davis, CA 95616, USA

OXFORD
UNIVERSITY PRESS

1

Quantum Phase Transitions

1.1 Introduction

Thermal phase transitions, usually triggered by fluctuations caused by tuning the temperature, T , close to some special value T_c , are very familiar daily phenomena. As the temperature is lowered, thermal fluctuations decrease and eventually will cease as $T \rightarrow 0$. As is well known, however, quantum fluctuations do not stop at zero temperature. These quantum fluctuations can, under certain conditions, trigger phase transitions known as quantum phase transitions (QPT). For this to happen, the amplitude of these fluctuations needs to be controlled which can be accomplished by tuning a parameter in the Hamiltonian governing the system. In what follows, we will present an introduction to these phase transitions with the help of two concrete examples which will serve to bring out some of the most important features and make clear the relation to classical statistical mechanics and thermal phase transitions.

We will start in this section with a brief review of thermal phase transitions, scaling relations and their generalization to QPT. We will then consider dynamics and its relation to excitation spectra. In section II we will present in some detail the specific example of the one-dimensional Ising model in a transverse magnetic field. In section III we will present the Hubbard model with a brief discussion of the main features of its phase diagram in the bosonic case. In addition, while this is not the focus of these lectures, we will, nonetheless, make contact between the formalism we will develop and the methods of Quantum Monte Carlo (QMC).

Our goal here is to present only a first pedagogical introduction to this interesting and important subject. For further study and application to other systems, we refer the reader to Refs. (Sachdev, 1999) and (Sondhi *et al.*, 1997).

1.1.1 Critical Points and Scaling Relations

Consider a lattice system at temperature $T = 0$ governed by a Hamiltonian of the form

$$\mathcal{H} = H_0 + gH_1. \tag{1.1}$$

where g is a tunable dimensionless parameter. If the lattice is finite and $[H_0, H_1] \neq 0$, then as g is tuned, there could be an avoided level crossing between the ground state and an excited state. As the system size increases, such an avoided level-crossing can sharpen and eventually, in the thermodynamic limit, become an actual level-crossing. When this happens, the energy, $E(g)$ (which is equal to the free energy, $F(g)$, since $T = 0$), becomes non-analytic at that value of g , signalling a phase transition. This is not a thermal but a quantum phase transition. A qualitative physical picture

of this QPT, which will be made more precise below, is as follows. H_0 and H_1 are competing terms which favor different quantum states. When $g \ll 1$, the ground state is dominated by H_0 with some perturbative quantum fluctuations caused by H_1 . When $g \gg 1$, the ground state is essentially that of H_1 . As g is tuned between these two extreme limits, the competition between H_0 and H_1 will determine the ground state and, at some value, g_c , the above mentioned level crossing may happen, indicating a QPT and a change in the relative dominance of H_0 and H_1 .

As for thermal phase transitions, a QPT can be continuous (for example second order) or discontinuous (first order). In these lectures we will focus exclusively on the case of second order transitions. It is well known that in the thermodynamic limit, second order thermal phase transitions in classical statistical physics are characterized by diverging quantities (Stanley, 1971; Ma, 1985; LeBellac *et al.*, 2004) such as the specific heat and the magnetic susceptibility. In particular, a very important diverging quantity is the correlation length, ξ , which exhibits the power law

$$\xi \sim |T - T_c|^{-\nu}, \quad (1.2)$$

where T_c is the critical temperature and ν is the *correlation length critical exponent*. The correlation length plays a crucial role near T_c since it sets the distance scale. For example, experiments show that near the transition, the Fourier transform of the correlation function (*i.e.* the structure factor) has the form (Stanley, 1971; Ma, 1985; LeBellac *et al.*, 2004)

$$\tilde{G}(|\vec{q}|) = \int d^D r e^{i\vec{q}\cdot\vec{r}} G(\vec{r}), \quad (1.3)$$

$$= \frac{1}{q^{2-\eta}} f(q\xi), \quad (1.4)$$

which defines the critical exponent η . Dimensional arguments then give the long distance behavior of the correlation function as

$$G(r) = \frac{1}{r^{D+\eta-2}} g\left(\frac{r}{\xi}\right). \quad (1.5)$$

The meaning of Eqs.(1.4) and (1.5) is that, near the critical point, the only characteristic length scale is the diverging correlation length, ξ . Equation (1.4) shows that in order for $\tilde{G}(|\vec{q}|)$ to be defined for $q = 0$, $f(q\xi) \sim (q\xi)^{2-\eta}$ as $q \rightarrow 0$ yielding

$$\tilde{G}(0) \sim \xi^{2-\eta} \sim |T - T_c|^{-\nu(2-\eta)}. \quad (1.6)$$

An example of $G(r)$ is the spin-spin correlation function. In such a case the magnetic susceptibility, which diverges as $\chi \sim |T - T_c|^{-\gamma}$, is proportional to $\tilde{G}(0)$ this gives the following relation between the critical exponents,

$$\gamma = \nu(2 - \eta). \quad (1.7)$$

Relation (1.7) is known as a *scaling relation*. Arguments similar to the above can be applied to other quantities such as the specific heat, $C \sim |T - T_c|^{-\alpha}$, the order

parameter, M , at T_c as a function of an external field, h , $M \sim h^{1/\delta}$ and the order parameter near T_c at $h = 0$, $M \sim |T - T_c|^{\tilde{\beta}}$. Such an analysis leads to the following scaling relations (Stanley, 1971; Ma, 1985; LeBellac *et al.*, 2004),

$$\alpha = 2 - \nu D, \quad 2\tilde{\beta} = \nu(D - 2 + \eta), \quad \delta = \frac{D + 2 - \eta}{D - 2 + \eta}. \quad (1.8)$$

The six critical exponents $(\alpha, \tilde{\beta}, \gamma, \delta, \nu, \eta)$ obey four scaling relations. Remark: the critical exponent $\tilde{\beta}$ traditionally has no tilde which we have added to avoid confusion with the inverse temperature β .

How is this modified by a QPT? To answer this question, we start with the partition function for a quantum system (Sachdev, 1999; LeBellac *et al.*, 2004),

$$Z = \text{Tr} e^{-\beta\mathcal{H}}, \quad (1.9)$$

where the Hamiltonian, \mathcal{H} , describes a D -dimensional quantum system. The expectation value of a quantum operator, \mathcal{O} , is given by

$$\langle \mathcal{O} \rangle = \frac{1}{Z} \text{Tr} \mathcal{O} e^{-\beta\mathcal{H}}. \quad (1.10)$$

Since the trace is an invariant, it can be evaluated in any representation and Eq.(1.9) can be written as

$$Z = \sum_{\{\phi\}} \langle \{\phi\} | e^{-\beta\mathcal{H}} | \{\phi\} \rangle, \quad (1.11)$$

where the $|\{\phi\}\rangle$ is a complete set of states. The operator $e^{-\beta\mathcal{H}}$ has the form of a quantum mechanical time evolution operator, $e^{-it\mathcal{H}}$, with $t \rightarrow -i\beta$. Equation (1.11) then lends itself to the following physical interpretation: The operator $e^{-\beta\mathcal{H}}$ evolves the state $|\{\phi\}\rangle$ by an imaginary time β ; the partition function is the sum of the amplitudes, matrix elements, of all “paths” that bring the system back to the original state. The return to the original state, *i.e.* periodic boundary conditions in the imaginary time direction, is imposed by the trace in Eq.(1.9). Taking the thermodynamic limit of the quantum system means that the extent of the system in the D space dimensions tends to infinity. Since we are interested in quantum phase transitions, we want to take $T \rightarrow 0$, in other words $\beta \rightarrow \infty$. This means that the system now has infinite extent in the original D space dimensions plus the new imaginary time direction: It has become effectively a $D + 1$ dimensional (classical) model. The details of this mapping will be worked out in the next section, for now we are only concerned with generalities. When the quantum critical point is approached, $g \rightarrow g_c$, the system will exhibit diverging quantities like in the thermal critical case. In particular, the correlation length in the space directions will diverge as (Sachdev, 1999)

$$\xi \sim |g - g_c|^{-\nu}. \quad (1.12)$$

The correlation “length”, ξ_τ , along the new imaginary time direction will also diverge but there is no *a priori* reason why it should diverge with the same exponent ν . In

general, for a second order QPT, we have (Sachdev, 1999; Hohenberg and Halperin, 1989)

$$\xi_\tau \sim \xi^z \sim |g - g_c|^{-\nu z}, \quad (1.13)$$

which defines the dynamic critical exponent z . We did not encounter this exponent in the thermal transitions of classical systems because they have no intrinsic dynamics. Equations (1.12) and (1.13) mean that the length scales in the space and imaginary time directions can, in general, be different, $z \neq 1$. Noting that ξ_τ has the same units as β , inverse energy, we see that the divergence of ξ_τ implies the vanishing of a characteristic energy. This is what happens when energy levels cross, as discussed above. We will see in section II an explicit example of such a vanishing energy scale.

The presence of the additional imaginary time dimension and a diverging correlation length along it will modify the scaling relations Eq.(1.8) which involve the dimensionality, D . Perhaps the first impulse is simply to replace D by $(D + 1)$ but this is not justified since the length scales are not necessarily the same in the new dimension. In fact, the same arguments which led to Eq.(1.5) will now lead to the following scaling form for the correlation function,

$$\begin{aligned} G(r, \tau) &\sim \frac{1}{s^{(D+z-2+\eta)}} g\left(\frac{r}{\xi}, \frac{\tau}{\xi_\tau}\right), \\ &\sim \frac{1}{s^{(D+z-2+\eta)}} g\left(\frac{r}{\xi}, \frac{\tau}{\xi^z}\right). \end{aligned} \quad (1.14)$$

where $s = \sqrt{r^2 + \tau^2}$ is the distance in space-imaginary time. We see that the effect of the added dimension is to add z rather than 1 to D ; this is reasonable since distances along the imaginary time direction are not measured in units of ξ but of ξ^z . Carrying these arguments forward generalizes the scaling relations Eq.(1.8) to yield (Fisher *et al.*, 1989),

$$\alpha = 2 - \nu(D + z), \quad 2\tilde{\beta} = \nu(D + z - 2 + \eta), \quad \delta = \frac{D + z + 2 - \eta}{D + z - 2 + \eta}. \quad (1.15)$$

The scaling relation Eq.(1.7) does not involve D and remains valid without any change. We see then that the commonly used statement “a D -dimensional quantum system is equivalent to a $(D + 1)$ -dimensional classical system”, while true, should be treated with care near a quantum critical point.

1.1.2 Dynamics and Excitation Energies

Consider a system in its ground state $|0\rangle$. The *dynamic correlation function* of an observable represented by an operator $\mathcal{O}(\vec{r}, t)$ is defined by

$$\begin{aligned} S(\vec{r}, \vec{r}', t) &= \langle 0 | \mathcal{O}^\dagger(\vec{r}, 0) \mathcal{O}(\vec{r}', t) | 0 \rangle, \\ &= \sum_m \langle 0 | \mathcal{O}^\dagger(\vec{r}, 0) | m \rangle \langle m | \mathcal{O}(\vec{r}', t) | 0 \rangle, \end{aligned} \quad (1.16)$$

where we inserted a complete set of energy eigenstates $1 = \sum |m\rangle \langle m|$ between the two operators. Recalling that

$$\mathcal{O}(\vec{r}', t) = e^{-i\mathcal{H}t} \mathcal{O}(\vec{r}', 0) e^{i\mathcal{H}t}, \quad (1.17)$$

where we take $\hbar = 1$. Eq.(1.16) becomes

$$\begin{aligned} S(\vec{r}, \vec{r}', t) &= \sum_m \langle 0 | \mathcal{O}^\dagger(\vec{r}, 0) | m \rangle \langle m | e^{-i\mathcal{H}t} \mathcal{O}(\vec{r}', 0) e^{i\mathcal{H}t} | 0 \rangle, \\ &= \sum_m e^{-i(E_m - E_0)t} \langle 0 | \mathcal{O}^\dagger(\vec{r}, 0) | m \rangle \langle m | \mathcal{O}(\vec{r}', 0) | 0 \rangle. \end{aligned} \quad (1.18)$$

We immediately see that the dynamic correlation function gives information about the excitation energies due to the appearance of $(E_m - E_0)$ in the exponential. Assuming that $S(\vec{r}, \vec{r}', \tau) = S(|\vec{r} - \vec{r}'|, \tau)$ and calculating its Fourier transform in space and time gives the dynamic structure factor

$$S(\vec{k}, \omega) = \sum_m \delta(\omega - E_m + E_0) |\langle 0 | \tilde{\mathcal{O}}(\vec{k}, 0) | m \rangle|^2 \quad (1.19)$$

We see that, for a given \vec{k} , $S(\vec{k}, \omega)$ is nonzero only when $\omega = E_m - E_0$. The dynamic structure factor is, therefore, a series of spikes whose height is given by $|\langle 0 | \tilde{\mathcal{O}}(\vec{k}, 0) | m \rangle|^2$ and whose position gives the excitation spectrum of the system.

However, as discussed above and shown in Eq.(1.11), the additional dimension we have here is imaginary time $t \rightarrow -i\beta$. Consequently, the dynamic structure factor will not exhibit oscillating complex exponentials as in Eq.(1.18) but rather exponential decay,

$$S(\vec{k}, \tau) = \sum_m e^{-(E_m - E_0)\tau} |\langle 0 | \tilde{\mathcal{O}}(\vec{k}, 0) | m \rangle|^2. \quad (1.20)$$

The first excited state is the slowest decaying one and, therefore, will dominate the exponential approach to the ground state contribution,

$$S(\vec{k}, \tau) \approx |\langle 0 | \tilde{\mathcal{O}}(\vec{k}, 0) | 0 \rangle|^2 + e^{-(E_1 - E_0)\tau} |\langle 0 | \tilde{\mathcal{O}}(\vec{k}, 0) | 1 \rangle|^2. \quad (1.21)$$

We see here a novel feature not present in classical thermal phase transitions namely the presence of a special direction, β , along which correlations can yield dynamical information. However, to access the excitation spectrum in this way, one needs the ‘‘Fourier transform in imaginary time’’ of the dynamical correlation function, *i.e.* its Laplace transform. If one has the functional form of the dynamical correlation function, it may be possible to calculate the Laplace transform without too much difficulty. However, one normally does not have this information. This is a situation where Quantum Monte Carlo (QMC) can help. If one evaluates $S(\vec{r}, \vec{r}', \tau)$ by means of QMC (see sections II and III), one can then implement a numerical Laplace transform, for example, using the Maximum Entropy method (Gubernatis *et al.*, 1991). The details of QMC and Maximum Entropy are beyond our scope here, they are mentioned as an example of how to exploit features of quantum critical phenomena absent in the classical case.

To end this section, we note that the exponential decay in Eq.(1.19) occurs only in the presence of an energy gap: $E_0 < E_1$. At a QCP where we have a level crossing, E_1

becomes equal to the ground state energy, E_0 , the gap and exponential decay disappear and power laws appear. We also note that the exponential decay in Eq.(1.21) can be written as $e^{-\tau/\xi_\tau}$ which makes explicit that the diverging correlation length in the imaginary time direction is due to a vanishing energy scale, $\xi_\tau \sim (E_1 - E_0)^{-1}$.

1.2 Quantum Ising Model

1.2.1 Generalities

The Ising model is, probably, the most familiar classical statistical model of magnetism (Stanley, 1971; Ma, 1985). Consider the sites i of a regular lattice on which we have classical “spins” $S_i = \pm 1$. The energy and partition function of the Ising model are

$$E = -J \sum_{\langle i,j \rangle} S_i S_j, \quad (1.22)$$

$$Z = \sum_{\{S_i\}} e^{\beta J \sum_{\langle i,j \rangle} S_i S_j}, \quad (1.23)$$

where β is the inverse temperature (we take Boltzmann’s constant $k_B = 1$), J is the coupling between the Ising spin variables and $\langle i, j \rangle$ denotes nearest neighbors. The sum over $\{S_i\}$ denotes a sum over all spin configurations. The properties of this model are well known and we will only discuss those we need as we proceed to the quantum case.

Now consider a system governed by the quantum Hamiltonian

$$\mathcal{H} = H_0 + H_1, \quad (1.24)$$

$$H_0 = -J \sum_{\langle i,j \rangle} \sigma_i^z \sigma_j^z, \quad (1.25)$$

$$H_1 = -h \sum_i \sigma_i^x, \quad (1.26)$$

where σ^x and σ^z are the usual Pauli matrices,

$$\sigma^x = \begin{pmatrix} 0 & 1 \\ 1 & 0 \end{pmatrix}, \quad \sigma^y = \begin{pmatrix} 0 & -i \\ i & 0 \end{pmatrix}, \quad \sigma^z = \begin{pmatrix} 1 & 0 \\ 0 & -1 \end{pmatrix}. \quad (1.27)$$

Equation (1.24) is the same as Eq.(1.1) but now with explicit forms for the non-commuting H_0 and H_1 . When $h = 0$ all the operators in the problem commute, and can be replaced by their eigenvalues, resulting in the classical Ising model. However, when $h \neq 0$, the non-commutativity $[H_0, H_1] \neq 0$, requires that we treat \mathcal{H} as a fully quantum system. While H_0 by itself is just the classical Ising model, H_1 describes an external magnetic field in the x direction and therefore transverse to the spin projections in H_0 . For this reason, Eq. 1.25 is referred to as the Ising model in a transverse field.

We will now consider the one-dimensional case of Eq.(1.24) in some detail to illustrate many of the points discussed in the previous section. We write

$$\mathcal{H} = -J \sum_{i=1}^N \sigma_{i+1}^z \sigma_i^z - h \sum_{i=1}^N \sigma_i^x, \quad (1.28)$$

where N is the total number of sites and we take periodic boundary conditions, $\sigma_{N+1}^z = \sigma_1^z$. The partition function is given by Eq.(1.9). Consider first the limiting case $h = 0$,

$$Z = \text{Tr} e^{\beta J \sum_{i=1}^N \sigma_{i+1}^z \sigma_i^z}. \quad (1.29)$$

To evaluate the trace, we use σ^z eigenvectors:

$$|+\rangle = \begin{pmatrix} 1 \\ 0 \end{pmatrix}, \quad |-\rangle = \begin{pmatrix} 0 \\ 1 \end{pmatrix} \quad (1.30)$$

with

$$\sigma^z |+\rangle = |+\rangle, \quad \sigma^z |-\rangle = -|-\rangle, \quad \sum_{S^z=\pm 1} |S^z\rangle \langle S^z| = 1 \quad (1.31)$$

The partition function becomes,

$$\begin{aligned} Z &= \left(\prod_{i=1}^N \sum_{S_i^z} \right) \left(\prod_{i=1}^N \langle S_i^z | \right) e^{\beta J \sum_{i=1}^N \sigma_{i+1}^z \sigma_i^z} \left(\prod_{i=1}^N |S_i^z\rangle \right) \\ &= \left(\prod_{i=1}^N \sum_{S_i^z} \right) \left(\prod_{i=1}^N \langle S_i^z | \right) e^{\beta J \sum_{i=1}^N S_{i+1}^z S_i^z} \left(\prod_{i=1}^N |S_i^z\rangle \right) \\ &= \sum_{\{S_i^z\}} \left(\prod_{i=1}^N \langle S_i^z | S_i^z \rangle \right) e^{\beta J \sum_{i=1}^N S_{i+1}^z S_i^z} \\ &= \sum_{\{S_i^z\}} e^{\beta J \sum_{i=1}^N S_{i+1}^z S_i^z} \end{aligned} \quad (1.32)$$

This is nothing but the partition function of the classical one-dimensional Ising model which can be easily solved and which has no phase transition at any finite temperature (LeBellac *et al.*, 2004). The other limiting case is to take $J = 0$,

$$Z = \text{Tr} e^{\beta h \sum_{i=1}^N \sigma_i^x} \quad (1.33)$$

Following the same steps which led to Eq.(1.32) but this time using eigenstates of σ^x ,

$$|\pm\rangle = \frac{1}{\sqrt{2}} \begin{pmatrix} 1 \\ \pm 1 \end{pmatrix}, \quad \sigma^x |+\rangle = |+\rangle, \quad \sigma^x |-\rangle = -|-\rangle, \quad (1.34)$$

leads to

$$Z = \prod_{i=1}^N \left[\sum_{S_i^x=\pm 1} e^{\beta h S_i^x} \right], \quad (1.35)$$

$$= [2 \cosh(\beta h)]^N, \quad (1.36)$$

which is nothing but the partition function of N independent spins. We, therefore, see that the two extreme limits, $h = 0$ and $J = 0$ lead back to classical cases.

1.2.2 Mapping to Classical System

Having both h and J nonzero leads to the interesting quantum critical behavior we seek. Several approaches to this problem are possible and here we demonstrate a general approach which can be applied essentially to any quantum model. The partition function of the full Hamiltonian governing the one-dimensional quantum system will be mapped onto that of a $(1 + 1)$ classical system as follows,

$$\begin{aligned} Z &= \text{Tr} e^{-\beta\mathcal{H}}, \\ &= \text{Tr} [e^{-\Delta\tau\mathcal{H}} e^{-\Delta\tau\mathcal{H}} e^{-\Delta\tau\mathcal{H}} \dots e^{-\Delta\tau\mathcal{H}} e^{-\Delta\tau\mathcal{H}}], \end{aligned} \quad (1.37)$$

where there are L exponentials in the product and $\beta = L\Delta\tau$ defines L and $\Delta\tau$. The product inside the trace can be viewed as a succession of imaginary time evolution operators. Note that no approximations were made in Eq.(1.37). Now, between each pair of exponentials, insert a complete set of σ_i^z eigenstates,

$$1 = \prod_{i=1}^N \left[\sum_{S_i^z = \pm 1} |S_i^z\rangle\langle S_i^z| \right], \quad (1.38)$$

$$\equiv \sum_{\{S_i^z\}} |S^z\rangle\langle S^z|. \quad (1.39)$$

Note that in Eq.(1.39) there is a complete set of eigenstates for every site which we then abbreviate with the notation of Eq.(1.39). Since we will make this insertion at several places along the string of exponentials, we will use a new index, ℓ , to label that position,

$$1 = \sum_{\{S_{i,\ell}^z\}} |S_\ell^z\rangle\langle S_\ell^z|. \quad (1.40)$$

The partition function then becomes,

$$Z = \sum_{\{S_{i,\ell} = \pm 1\}} \langle S_1^z | e^{-\Delta\tau\mathcal{H}} | S_L^z \rangle \langle S_L^z | e^{-\Delta\tau\mathcal{H}} | S_{L-1}^z \rangle \langle S_{L-1}^z | e^{-\Delta\tau\mathcal{H}} | S_{L-2}^z \rangle \dots \quad (1.41)$$

$$\dots \langle S_3^z | e^{-\Delta\tau\mathcal{H}} | S_2^z \rangle \langle S_2^z | e^{-\Delta\tau\mathcal{H}} | S_1^z \rangle \quad (1.42)$$

Since Z is a trace, we have the same state at the beginning and end of the chain. As we discussed for Eq.(1.11), $e^{-\Delta\tau\mathcal{H}}$ is an evolution operator in imaginary time for a step of $\Delta\tau$. The partition function has become a product of matrix elements each representing the evolution of the quantum mechanical state from “imaginary time slice” ℓ to “imaginary time slice” $\ell + 1$. It now remains to evaluate these matrix elements which is where we will make our first approximation,

$$\begin{aligned} \langle S_{\ell+1}^z | e^{-\Delta\tau\mathcal{H}} | S_\ell^z \rangle &= \langle S_{\ell+1}^z | e^{-\Delta\tau H_1 - \Delta\tau H_0} | S_\ell^z \rangle \\ &\approx \langle S_{\ell+1}^z | (e^{-\Delta\tau H_1} e^{-\Delta\tau H_0} + \mathcal{O}(\varepsilon)) | S_\ell^z \rangle. \end{aligned} \quad (1.43)$$

$\mathcal{O}(\varepsilon)$ is the Trotter error and is of order $(\Delta\tau)^2 Jh$ as can be seen from

$$\varepsilon = [\Delta\tau H_0, \Delta\tau H_1] = (\Delta\tau)^2 [H_0, H_1] = \mathcal{O}((\Delta\tau)^2 Jh). \quad (1.44)$$

This approximation, called the Trotter-Suzuki approximation, is controlled in the sense that one can get as close to the exact result as one desires by requiring that

$$\begin{aligned} (\Delta\tau)^2 Jh &\ll 1, \\ L^2 &\gg \beta^2 Jh, \\ L &\gg \beta\sqrt{Jh}. \end{aligned} \quad (1.45)$$

In other words, we have divided β into L time slices to make $\Delta\tau$ small, justifying the Trotter-Suzuki approximation and allowing us to evaluate the matrix elements. It is very important to keep in mind that, regardless of the value of L , this is *not* a perturbative calculation: Non-perturbative effects are all present in this formalism.

The matrix element, Eq.(1.43), can now be evaluated easily by noting that the exponential of H_0 (see Eq.(1.25)) acts on σ^z eigenstates on the right giving,

$$\begin{aligned} \langle S_{\ell+1}^z | e^{-\Delta\tau H_1} e^{-\Delta\tau H_0} | S_\ell^z \rangle &= \langle S_{\ell+1}^z | e^{-\Delta\tau H_1} e^{\Delta\tau J \sum_{i=1}^N S_{i,\ell}^z S_{i+1,\ell}^z} | S_\ell^z \rangle \\ &= e^{\Delta\tau J \sum_{i=1}^N S_{i,\ell}^z S_{i+1,\ell}^z} \langle S_{\ell+1}^z | e^{\Delta\tau h \sum_{i=1}^N \sigma_i^x} | S_\ell^z \rangle \end{aligned} \quad (1.46)$$

To calculate the remaining matrix element we note that since $\sigma_x^2 = 1$, the identity matrix, then

$$e^{\Delta\tau h \sigma_x} = 1 \cosh(\Delta\tau h) + \sigma_x \sinh(\Delta\tau h). \quad (1.47)$$

We require that the matrix element be expressed in the form

$$\langle S'_z | e^{\Delta\tau h \sigma_x} | S_z \rangle \equiv \Lambda e^{\gamma S'_z S_z}, \quad (1.48)$$

which defines Λ and γ . To determine Λ and γ , we calculate Eq.(1.48), using Eq.(1.47), for the two cases $S_z = S'_z$ and $S_z = -S'_z$,

$$\langle S_z | e^{\Delta\tau h \sigma_x} | S_z \rangle = \cosh(\Delta\tau h) = \Lambda e^\gamma, \quad (1.49)$$

$$\langle -S_z | e^{\Delta\tau h \sigma_x} | S_z \rangle = \sinh(\Delta\tau h) = \Lambda e^{-\gamma}, \quad (1.50)$$

which yield,

$$\gamma = -\frac{1}{2} \ln \tanh(\Delta\tau h). \quad (1.51)$$

$$\Lambda^2 = \sinh(\Delta\tau h) \cosh(\Delta\tau h) \quad (1.52)$$

Equation (1.46) then becomes,

$$\langle S_{\ell+1}^z | e^{-\Delta\tau H_1} e^{-\Delta\tau H_0} | S_\ell^z \rangle = \Lambda^N e^{\Delta\tau J \sum_{i=1}^N S_{i,\ell}^z S_{i+1,\ell}^z + \gamma \sum_{i=1}^N S_{i,\ell}^z S_{i,\ell+1}^z}. \quad (1.53)$$

Note that in Eq.(1.53), H_0 led to Ising spin couplings at the same imaginary time slice but near neighbor spatial sites while H_1 led to couplings between Ising spins on the

xiv Quantum Phase Transitions

same spatial site but “near neighbor” (consecutive) imaginary time slices. Substituting Eq.(1.53) in Eq.(1.42) finally yields,

$$Z = \Lambda^{NL} \sum_{\{S_{i,\ell}=\pm 1\}} e^{\Delta\tau J \sum_{i=1}^N \sum_{\ell=1}^L S_{i,\ell} S_{i+1,\ell} + \gamma \sum_{i=1}^N \sum_{\ell=1}^L S_{i,\ell} S_{i,\ell+1}}, \quad (1.54)$$

where $\gamma > 0$ is given by Eq.(1.51) and where we dropped the z superscript on the spins. The prefactor, Λ^{NL} , is not important because it does not affect the spins and therefore does not affect the transition. In addition, this prefactor cancels out when average values of physical quantities are calculated. Eq.(1.54) is nothing but the partition function of the classical $D = 2$ Ising model, Eq.(1.23), with different couplings in the i and ℓ directions,

$$Z_{cl} = \sum_{\{S_{i,\ell}=\pm 1\}} e^{\beta_{cl} J_x \sum_{i=1}^{N_x} \sum_{j=1}^{N_y} S_{i,j} S_{i+1,j} + \beta_{cl} J_y \sum_{i=1}^{N_x} \sum_{j=1}^{N_y} S_{i,j} S_{i,j+1}}. \quad (1.55)$$

We then identify,

$$\begin{aligned} N_x &= N \\ N_y &= L \\ \beta_{cl} J_x &= \Delta\tau J \\ \beta_{cl} J_y &= \gamma \end{aligned} \quad (1.56)$$

The one-dimensional Ising model in a transverse field is thus mapped onto a classical $(1 + 1)$ dimensional Ising model with anisotropic couplings. Note that β_{cl} is not the inverse temperature of the original quantum system, $\beta = L\Delta\tau$.

1.2.3 Quantum Phase Transition

The classical two dimensional Ising model, Eq.(1.55), can be solved exactly in the absence of an external magnetic field (Onsager, 1944; Baxter, 1982). It is known that in the thermodynamic limit, $N_x \rightarrow \infty$ and $N_y \rightarrow \infty$, this system has a critical point given by the relation (which can also be obtained using the duality transformation (Baxter, 1982; Kramers and Wannier, 1941; Savit, 1980))

$$\sinh(2J_x\beta_{cl}^c) \sinh(2J_y\beta_{cl}^c) = 1, \quad (1.57)$$

where β_{cl}^c is the critical inverse temperature for the classical system. For low temperature, $\beta_{cl} > \beta_{cl}^c$, the system is ordered (magnetized) while for high temperature, $\beta_{cl} < \beta_{cl}^c$, the system is disordered. While the value of β_{cl}^c depends on the relative values of J_x and J_y , *i.e.* on the anisotropy, the critical exponents themselves do not (Onsager, 1944): The critical points for all J_x/J_y are in the same universality class. For $J_x = J_y$ Eq.(1.57) yields $2J_x\beta_{cl}^c = \ln(1 + \sqrt{2})$.

With the mapping of the $D = 1$ quantum system to the $(1 + 1)$ classical system, Eq.(1.54), and the parameter identification Eq.(1.56), we, therefore, see that as $N \rightarrow \infty$ and $L \rightarrow \infty$ the quantum system will exhibit a critical point given by the condition

$$\sinh(2J^c \Delta\tau) \sinh(2\gamma^c) = 1, \quad \gamma^c = -\frac{1}{2} \ln \tanh(h^c \Delta\tau). \quad (1.58)$$

This, however, is not a thermal phase transition since it takes place when the quantum system is at zero temperature. We see this by noting that for the transition to take place, both $N \rightarrow \infty$ and $L \rightarrow \infty$. But when $L \rightarrow \infty$ at fixed $\Delta\tau$, which is the case here, it means that $\beta \rightarrow \infty$ and thus the system is at $T = 0$. We have here, therefore, a quantum phase transition reached by tuning J and h , the coupling parameters while the system is at zero temperature. Equation (1.58) serves to get the critical point. Substituting the expression for γ^c in the condition for criticality, Eq.(1.58), yields

$$\begin{aligned} 1 &= \frac{1}{2} \sinh(2J^c \Delta\tau) \left(\frac{\cosh(h^c \Delta\tau)}{\sinh(h^c \Delta\tau)} - \frac{\sinh(h^c \Delta\tau)}{\cosh(h^c \Delta\tau)} \right) \\ &= \sinh(2J^c \Delta\tau) \left(\frac{\cosh^2(h^c \Delta\tau) - \sinh^2(h^c \Delta\tau)}{2 \cosh(h^c \Delta\tau) \sinh(h^c \Delta\tau)} \right) \\ &= \frac{\sinh(2J^c \Delta\tau)}{\sinh(2h^c \Delta\tau)} \end{aligned} \quad (1.59)$$

Putting $h = gJ$, we see that Eq.(1.59) is satisfied for any J^c as long as $g^c = 1$. We therefore conclude that the $D = 1$ Ising model in a transverse field, undergoes a quantum phase transition, i.e. at $T = 0$, at the critical coupling $g^c = 1$.

As we saw in the introduction, Eq.(1.13), the correlation length along the imaginary time direction diverges as $\xi_\tau \sim \xi^z$. But it is known for the anisotropic Ising model that rotational isotropy is restored at the critical point: The system looks and behaves the same in all directions. Therefore, in our effective $(1 + 1)$ model, $\xi_\tau \sim \xi$ at the quantum critical point. Consequently, for the $D = 1$ Ising model in transverse field we have the dynamic critical exponent $z = 1$. All the other exponents, α , β , γ , δ , η and ν have the same values as the classical $D = 2$ model. This is, perhaps, not hard to understand qualitatively: The couplings in Eq.(1.54) have the same form in the x and β directions, only the details are somewhat different, so when the correlations diverge it is not unreasonable that the system behave in the same way in both directions. This is not true for all quantum models as we will see in the next section.

Applying the above to the isotropic $D = 2$ Ising model in a transverse field at inverse temperature β , we obtain the mapping to the $(2 + 1)$ dimensional classical model with equal couplings in the x and y directions but different couplings in the β direction. The QPT is obtained in the same way: $N_x \rightarrow \infty$, $N_y \rightarrow \infty$ and $L \rightarrow \infty$ (with $\Delta\tau$ constant). This system will undergo a quantum phase transition, in the thermodynamic and $\beta \rightarrow \infty$ limits, at parameter values which are not known exactly but which can be estimated, for example, numerically.

Again, near the transition, isotropy is restored which gives $z = 1$.

Practice problem: A good practice problem is to apply the above to the Hamiltonian

$$\mathcal{H} = -J\sigma^z - h\sigma^x, \quad (1.60)$$

which represents a ($D = 0$) single Ising variable in a transverse field. This Hamiltonian will lead to the $(0 + 1)$ dimensional classical Ising model which can be solved trivially.

Although this model does not have a phase transition, the exercise is, nonetheless, very instructive.

1.2.4 Discussion

- It is important not to confuse β , the inverse temperature of the quantum system, with β_{cl} ; see for example Eqs. (1.54), (1.55), (1.57) and (1.58). β is the true inverse temperature of the quantum system and, after the mapping to the $(D+1)$ classical system, manifests itself only through $\Delta\tau$ and L .
- The following point, which was discussed above, is worth re-iterating. The fact that we needed to take $\Delta\tau$ “very small” (actually $(\Delta\tau)^2 Jh \ll 1$) does not mean that the results are perturbative. We needed this condition only to be able to evaluate the matrix elements at each imaginary time slice. All nonperturbative effects are included.
- The mapping which took the one-dimensional quantum system to a two-dimensional “classical” system is rather general. Details of the mapping, such as evaluation of the matrix elements, will depend on the model but the general approach is the same: Any D -dimensional quantum system can, through a similar succession of steps, be mapped onto an equivalent $(D+1)$ -dimensional classical model. The additional dimension, β , is interpreted as the “imaginary time” direction. We will see another example below.
- If one wants to simulate numerically a quantum system, one can first map it onto its equivalent $(D+1)$ -dimensional classical equivalent and perform a classical simulation on the resulting system. This is known as the Quantum Monte Carlo method. One should, however, be careful with the observables: It is not always obvious what form a quantum observable takes in the equivalent classical model in $(D+1)$ dimensions. However, the new form can be found by performing the same mapping on the expectation value, Eq.(1.10), as on the partition function (LeBellac *et al.*, 2004; Hirsch *et al.*, 1992; Batrouni and Scalettar, 1992; Tobochnik *et al.*, 1992).
- We have seen that the path integral for the $D = 1$ Ising model in transverse field led to the $D = 2$ classical Ising model, for which we have Onsager’s exact solution. It should not be surprising, then, that the transverse Ising model should have a direct analytic treatment.

Indeed, an elegant and direct solution is found with the Jordan-Wigner transformation (see appendix) which can map a 1-dimensional spin system onto a 1-dimensional noninteracting fermionic system. The Hamiltonian for a noninteracting system can be easily diagonalized to yield the energy spectrum. For the Hamiltonian Eq.(1.24) one obtains

$$\epsilon(k) = 2J (1 + g^2 - 2g\cos(k))^{1/2}, \quad (1.61)$$

where k is the wave vector, $p = \hbar k$. The lowest excitation (*i.e.* gap) energy is for $k = 0$, $\epsilon(0) = 2J|1 - g|$ which gives $g_c = 1$, in agreement with Eq.(1.59). We can then write,

$$\epsilon(0) = 2J|g - g_c|. \quad (1.62)$$

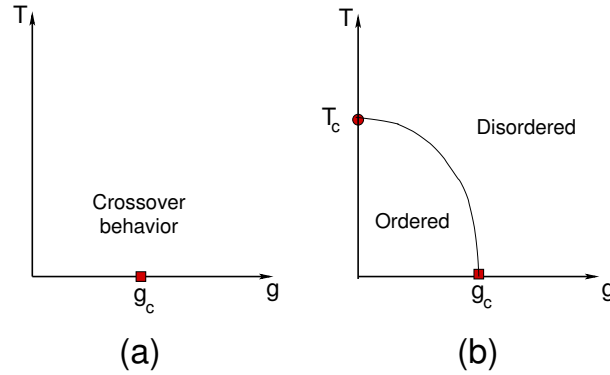


Fig. 1.1 (a) Schematic of the phase diagram of the 1-dimensional quantum Ising model in the temperature-coupling space. The square denotes the quantum critical point. (b) The phase diagram for the 2-dimensional case. The square denote a quantum phase transition and the circle a thermal one; the two are connected by a line of thermal critical points.

At the end of Section I we said that $\xi_\tau \sim (E_1 - E_0)^{-1}$ which, because of Eq.(1.62), becomes $\xi_\tau \sim |g - g_c|^{-1}$. Therefore Eq.(1.13) gives $\nu z = 1$ and, since $\nu = 1$ for the classical two-dimensional Ising model, we obtain again $z = 1$.

The Jordan-Wigner transformation applies only in one dimension, so this method cannot be used, for example, to solve the 2-dimensional Ising model in a transverse field.

- What happens to the QPT at finite temperature? At finite T there are thermal fluctuations which tend to drive the phase transition, *if there is one*.

For example, the $D = 1$ Ising model in a transverse field has a QPT at $T = 0$ for $g_c = 1$. We also saw, Eq.(1.29) to (1.32), that, when $h = 0$ (and therefore $g = 0$), this model is simply the classical one-dimensional Ising chain which exhibits no phase transition at any temperature. At finite T , L is finite and therefore when $N \rightarrow \infty$, the partition function Eq.(1.54) describes an infinite strip and consequently the system is effectively one-dimensional and will not exhibit any phase transitions. Its phase diagram will, therefore, be like Fig.1.1(a).

Now consider the $D = 2$ Ising model in a transverse field. When $T = 0$, there is a QPT at g_c , as discussed above. In addition, however, when $h = 0$ (i.e. $g = 0$) the system becomes the two-dimensional classical Ising model which exhibits a thermal second order phase transition at $T/J = 2.2691 \dots$. So, there is a quantum phase transition at $(g_c, T = 0)$ and a *thermal* one at $(g = 0, T_c)$. These two transitions are typically connected by a line of thermal critical points as illustrated in Fig.1.1(b).

1.3 Hubbard Model

What has become known as “the Hubbard model” covers a rather large class of models, both bosonic and fermionic. These models play a central role in the study of strongly correlated systems exhibiting a very wide range of quantum phases and quantum

phase transitions. A partial list of phases exhibited by these systems include high temperature superconductivity, superfluidity, supersolids, antiferromagnetism, Mott insulator, Bose glasses, ultra cold atoms loaded on optical lattices etc (Fazekas, 1999; Rasetti, 1991).

The original model (Gutzwiller, 1963; Hubbard, 1964; Kanamori, 1963), used to study magnetic transitions, described fermions on a square lattice governed by the Hamiltonian

$$\mathcal{H} = -t \sum_{\langle ij \rangle \sigma} (c_{i\sigma}^\dagger c_{j\sigma} + c_{j\sigma}^\dagger c_{i\sigma}) + U \sum_i \left(\hat{n}_{i\uparrow} - \frac{1}{2} \right) \left(\hat{n}_{i\downarrow} - \frac{1}{2} \right) - \mu \sum_i (\hat{n}_{i\uparrow} + \hat{n}_{i\downarrow}). \quad (1.63)$$

$c_{i\sigma}$ and $c_{i\sigma}^\dagger$ are destruction and creation operators of fermions with spin $\sigma = \uparrow, \downarrow$ on site i and they satisfy the anti-commutation relations

$$\{c_{i\sigma}^\dagger, c_{j\sigma'}\} = \delta_{i,j} \delta_{\sigma,\sigma'}, \quad \{c_{i\sigma}, c_{j\sigma'}\} = \{c_{i\sigma}^\dagger, c_{j\sigma'}^\dagger\} = 0. \quad (1.64)$$

Therefore, the first term in Eq.(1.63) is the kinetic energy term governing how fermions jump between near neighbor sites, $\langle ij \rangle$. t is called the hopping parameter and by making contact with the kinetic energy in the Schrödinger equation, we can identify $t = \hbar^2/2m$. The contact interaction is described by the second term where U is the interaction strength and $\hat{n}_{i\sigma} = c_{i\sigma}^\dagger c_{i\sigma}$ is the number operator on site i . The chemical potential μ controls the particle population in the grand canonical ensemble.

A natural generalization of the above model is to consider the properties of a system of bosons on a lattice governed by a similar Hamiltonian (Fisher *et al.*, 1989),

$$\mathcal{H} = -t \sum_{\langle i,j \rangle} (a_i^\dagger a_j + a_j^\dagger a_i) + \frac{U}{2} \sum_i \hat{n}_i (\hat{n}_i - 1) - \mu \sum_i \hat{n}_i, \quad (1.65)$$

where the bosonic operators satisfy

$$[a_i, a_j^\dagger] = \delta_{i,j}, \quad [a_i^\dagger, a_j^\dagger] = [a_i, a_j] = 0. \quad (1.66)$$

In Eq.(1.65) we considered the simplest case of spin-0 bosons but one can also consider bosons of higher spins. In both Eqs.(1.63) and (1.65) we only included contact interactions. However, both models have been extended to include nearest and next nearest neighbors (Niyaz *et al.*, 1991; Niyaz *et al.*, 1994; Batrouni and Scalettar, 2000) and even longer range interactions and disorder (Fisher *et al.*, 1989). Such additional interactions vastly enrich the phase diagrams of these models and introduce new exotic phases of which we mentioned a few at the beginning of this section.

Although, initially, interest in these models was focused on condensed matter issues, this focus recently widened considerably with the experimental realization of atomic Bose-Einstein Condensates (BEC). It was shown that if one produces a standing wave with pairs of counter-propagating laser beams (called an “optical lattice”) and then loads ultra-cold fermionic or bosonic atoms on this optical lattice, the resulting system is, indeed, governed by Eqs.(1.63) or (1.65) with *experimentally tunable* interaction strength and range (Jaksch *et al.*, 1998). In addition, the optical lattices can be made in

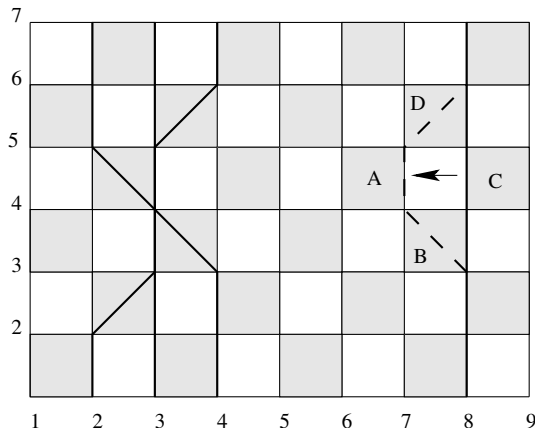


Fig. 1.2 The decomposition of the full Hamiltonian \mathcal{H} into H_1 and H_2 results in a “checkerboard” pattern for the space-imaginary time lattice. Periodic boundary conditions are used in space, so that on this 8-site lattice, site 1 is identified with site 9. Furthermore, the trace in the partition function imposes periodic boundary conditions in the imaginary time direction so that world lines have to close on themselves. Only for even time slices are bosons allowed to hop between sites (2, 3), (4, 5), (6, 7), ..., while only for odd time slices can they hop between sites (1, 2), (3, 4), ... The bold paths are boson world lines, the arrow shows a typical allowed deformation.

1, 2, and 3 dimensions. This high degree of experimental flexibility and control allows detailed comparisons between the physics of strongly correlated systems governed by Hamiltonians of the Hubbard type, Eq.(1.63, 1.65), and those realized experimentally. This is currently a very active field with new experimental and theoretical/numerical results appearing very frequently.

In these lectures we will concentrate on the phase diagram and the quantum phase transitions of the spin-0 bosonic Hubbard model governed by Eq.(1.65).

1.3.1 Mapping to Classical System

The mapping of the Hubbard model onto a classical model proceeds along a path similar to that for the Ising model in a transverse field. We will, nonetheless, show it in some detail in order to fix ideas and to emphasize that, unlike the Ising case, the classical model can be unfamiliar and not correspond to a well studied model.

To implement the mapping, we consider the one-dimensional version of Eq.(1.65),

$$\mathcal{H} = -t \sum_{i=1}^N \left(a_i^\dagger a_{i+1} + a_{i+1}^\dagger a_i \right) + \frac{U}{2} \sum_{i=1}^N \hat{n}_i (\hat{n}_i - 1) - \mu \sum_{i=1}^N \hat{n}_i, \quad (1.67)$$

where N is the number of sites and we take periodic boundary conditions, $a_{N+1} = a_1$. As for the Ising case, we start with the partition function,

$$\begin{aligned} Z &= \text{Tr} e^{-\beta \mathcal{H}}, \\ &= \text{Tr} \left[e^{-\Delta\tau \mathcal{H}} e^{-\Delta\tau \mathcal{H}} e^{-\Delta\tau \mathcal{H}} \dots e^{-\Delta\tau \mathcal{H}} e^{-\Delta\tau \mathcal{H}} \right], \end{aligned} \quad (1.68)$$

where there are L terms in the product and, as before, $\beta = L\Delta\tau$. There are several representations possible to calculate the trace. We will choose the occupation number representation, $|\mathbf{n}\rangle \equiv |n_1, n_2, \dots, n_i, \dots, n_N\rangle$ where

$$a_i^\dagger |n_1, n_2, \dots, n_i, \dots, n_N\rangle = \sqrt{n_i + 1} |n_1, n_2, \dots, n_i + 1, \dots, n_N\rangle, \quad (1.69)$$

$$a_i |n_1, n_2, \dots, n_i, \dots, n_N\rangle = \sqrt{n_i} |n_1, n_2, \dots, n_i - 1, \dots, n_N\rangle, \quad (1.70)$$

$$\hat{n}_i |n_1, n_2, \dots, n_i, \dots, n_N\rangle = n_i |n_1, n_2, \dots, n_i, \dots, n_N\rangle, \quad (1.71)$$

$$(1.72)$$

and the completeness condition,

$$\sum_{\{\mathbf{n}\}} |\mathbf{n}\rangle \langle \mathbf{n}| \equiv \left(\prod_{i=1}^N \sum_{n_i=0}^{\infty} \right) |n_1, n_2, \dots, n_N\rangle \langle n_1, n_2, \dots, n_N| = 1. \quad (1.73)$$

This representation has the advantage of being very familiar and will lead to a partition function amenable to intuitive physical representation. Before inserting complete sets of state in Eq.(1.68), we will choose to work in the canonical ensemble where the total number of particles is fixed and, therefore, the chemical potential term is not present. We will also split the Hamiltonian, as follows,

$$\begin{aligned} \mathcal{H} &= H_1 + H_2 \\ H_1 &= -t \sum_{i=odd} \left(a_i^\dagger a_{i+1} + a_{i+1}^\dagger a_i \right) + \frac{U}{4} \sum_{i=1}^N \hat{n}_i (\hat{n}_i - 1), \\ H_2 &= -t \sum_{i=even} \left(a_i^\dagger a_{i+1} + a_{i+1}^\dagger a_i \right) + \frac{U}{4} \sum_{i=1}^N \hat{n}_i (\hat{n}_i - 1). \end{aligned} \quad (1.74)$$

This splitting of \mathcal{H} means that the hopping term in H_1 connects sites (1, 2), (3, 4), (5, 6) etc. while H_2 connects sites (2, 3), (4, 5), (6, 7) etc. It is called the ‘‘checkerboard decomposition’’ for reasons that will become clear shortly (Hirsch *et al.*, 1992). Notice that the interaction term was divided equally between H_1 and H_2 . We then have,

$$e^{-\Delta\tau H} \approx e^{-\Delta\tau H_1} e^{-\Delta\tau H_2} + \mathcal{O}(\varepsilon), \quad (1.75)$$

where

$$\varepsilon = [\Delta\tau H_1, \Delta\tau H_2] = (\Delta\tau)^2 [H_1, H_2] = \mathcal{O}((\Delta\tau)^2 tU). \quad (1.76)$$

Once again, we find that for this procedure to be accurate, one needs to take a large enough number of time slices, L , to make $(\Delta\tau)^2 Ut \ll 1$. Now insert Eq.(1.75) in Eq.(1.68) and insert between each pair of exponentials a complete set of states, Eq.(1.73). This yields,

$$Z = \sum_{\{\mathbf{n}\}} \langle \mathbf{n}^1 | e^{-\Delta\tau H_2} | \mathbf{n}^{2L} \rangle \langle \mathbf{n}^{2L} | e^{-\Delta\tau H_1} | \mathbf{n}^{2L-1} \rangle \dots \langle \mathbf{n}^3 | e^{-\Delta\tau H_2} | \mathbf{n}^2 \rangle \langle \mathbf{n}^2 | e^{-\Delta\tau H_1} | \mathbf{n}^1 \rangle. \quad (1.77)$$

The partition function is now expressed as a path integral, Eq.(1.77), with an appealing intuitive geometrical interpretation in terms of *world lines*, i.e. the paths traced

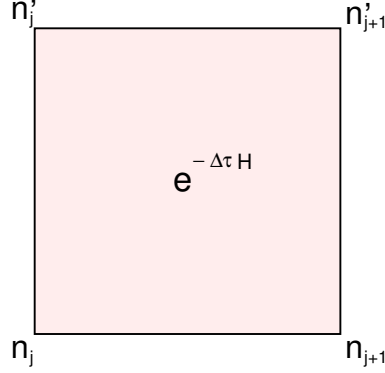


Fig. 1.3 An elementary matrix element represented by shaded squares in Fig. 1.2.

by the bosons as they evolve in space-imaginary time (Hirsch *et al.*, 1992). To see this, consider, for example, the matrix element $\langle \mathbf{n}^2 | e^{-\Delta\tau H_1} | \mathbf{n}^1 \rangle$: As is clear from its definition, Eqs.(1.74), the hopping term (kinetic energy) in H_1 couples only the pairs (1, 2), (3, 4), (5, 6) *etc.* but not the pairs (2, 3), (4, 5), (6, 7) *etc.*, which are connected by H_2 . Consequently, the matrix elements of $e^{-\Delta\tau H_1}$ are products of *independent* two-site problems: (1, 2), (3, 4), (5, 6) ... Similarly, a matrix element of $\exp(-\Delta\tau H_2)$ is a product of independent two-site problems (2, 3), (4, 5), (6, 7) ... This is shown in figure 1.2 where the shaded squares represent the imaginary-time evolution of connected pairs. The thick lines represent a possible configuration of boson world lines traced by the particles initially present at the first time slice as the imaginary time evolution operators evolve the state from one time slice to the next. Because of the checkerboard division of $\mathcal{H} = H_1 + H_2$, a boson can jump only across a shaded square.

The matrix element represented by a shaded square can now be calculated easily. Consider such a square at time slice where, for example, H_1 acts (see Fig.1.3),

$$\begin{aligned} \langle n'_j, n'_{j+1} | e^{-\Delta\tau H_1} | n_j, n_{j+1} \rangle &\approx \langle n'_j, n'_{j+1} | e^{-\Delta\tau \hat{U}/2} e^{\Delta\tau t(a_j^\dagger a_{j+1} + a_{j+1}^\dagger a_j)} e^{-\Delta\tau \hat{U}/2} | n_j, n_{j+1} \rangle, \\ &= e^{-\Delta\tau \mathcal{U}'/2} e^{-\Delta\tau \mathcal{U}/2} \\ &\quad \times \langle n'_j, n'_{j+1} | e^{\Delta\tau t(a_j^\dagger a_{j+1} + a_{j+1}^\dagger a_j)} | n_j, n_{j+1} \rangle, \end{aligned} \quad (1.78)$$

where

$$\begin{aligned} \mathcal{U} &= \frac{U}{4} (n_j(n_j + 1) + n_{j+1}(n_{j+1} + 1)), \\ \mathcal{U}' &= \frac{U}{4} (n'_j(n'_j + 1) + n'_{j+1}(n'_{j+1} + 1)). \end{aligned} \quad (1.79)$$

The remaining matrix element in Eq.(1.78) is easy to calculate by expanding the exponential in powers of $(\Delta\tau)$, but can also be calculated exactly (LeBellac *et al.*, 2004). It vanishes unless $n_j + n_{j+1} = n'_j + n'_{j+1}$ and is positive when this condition is satisfied.

The partition function of the one-dimensional bosonic Hubbard model is, therefore, expressed as a “path integral” which is the sum over all conformations and deformations of N_b lines where N_b is the number of bosons. The partition function of the two-dimensional system can be represented in a similar manner but in this case there are more intricate configurations possible. For example, boson world lines can wrap around each other forming a helical structure.

We remark that all the matrix elements in Eq.(1.77) are real and positive (for the bosonic model in the absence of frustration). Consequently, this world line representation forms the basis for many quantum Monte Carlo algorithms applied to a wide class of bosonic and magnetic systems (Hirsch *et al.*, 1992; Batrouni and Scalettar, 1992; Tobochnik *et al.*, 1992; Prokof'ev *et al.*, 1998).

This mapping of the quantum system onto a classical system of interacting extended objects (lines) can be exploited by using known properties of the quantum system to understand those of classical extended objects. For example, this was used to understand the properties of interstitials and vacancies and argue for supersolid order in vortex crystals (Frey *et al.*, 1994). In this case, understanding the quantum system shed light on the behavior of a classical system.

Notice that it is clear with this representation that, unlike the example of the quantum Ising model, the space and imaginary time directions are not equivalent. One way to see this is as follows: World lines can hop in the positive or negative space directions, but they can only hop in the positive imaginary time direction!

Practice problem: There are other useful representations for expressing the partition function as a path integral. A very useful representation is in terms of coherent states, eigenstates of the destruction operator,

$$a_i|\{\Phi\}\rangle = \phi(i)|\{\Phi\}\rangle, \quad \langle\{\Phi\}|a_i^\dagger = \langle\{\Phi\}|\phi^*(i) \quad (1.80)$$

where the eigenvalues $\phi(i)$ are complex numbers that are defined on the sites, i , of the lattice. In terms of the more familiar occupation number representation vacuum ($a|0\rangle = 0, a^\dagger|0\rangle = |1\rangle$) the coherent state $|\Phi\rangle$ is defined as follows (Negele and Orland, 1998; Gardiner, 2009).

$$|\{\Phi\}\rangle = \exp\left(\sum_i\left(-\frac{1}{2}\phi^*(i)\phi(i) + \phi(i)a_i^\dagger\right)\right)|0\rangle. \quad (1.81)$$

With this normalization we obtain the inner product of two coherent states

$$\langle\{\Psi\}|\{\Phi\}\rangle = \exp\left(\sum_i\left(\psi^*(i)\phi(i) - \frac{1}{2}\phi^*(i)\phi(i) - \frac{1}{2}\psi^*(i)\psi(i)\right)\right), \quad (1.82)$$

and the resolution of unity

$$1 = \int \prod_i \frac{d^2\phi(i)}{2\pi} |\{\Phi\}\rangle\langle\{\Phi\}|. \quad (1.83)$$

Use this representation to evaluate the trace in Eq.(1.68) and express the partition function as the path integral,

$$Z = \int \prod_{i,\ell} \frac{d^2\phi(i,\ell)}{\pi} e^{-S(\phi^*,\phi)}, \quad (1.84)$$

where the action is given by (Batrouni and Mabilat, 1999)

$$S = \sum_{i,\ell} \phi^*(i,\ell) \Delta_{-\tau} \phi(i,\ell) + \Delta\tau \sum_{\ell} \mathcal{H}[\phi^*(i,\ell+1), \phi(i,\ell)], \quad (1.85)$$

and where i is the spatial index of the site and ℓ the imaginary time slice. In Eq.(1.85), $\mathcal{H}[\phi^*(i,\ell), \phi(i,\ell-1)]$ means that at the imaginary time slice ℓ , we replace in the Hamiltonian, Eq.(1.65), the destruction operator a_i by the complex field $\phi(i,\ell)$, and the creation operator, a_i^\dagger , by $\phi^*(i,\ell+1)$. Furthermore, the forward and backward finite difference operators are

$$\Delta_{\tau} \phi(i,\ell) \equiv \phi(i,\ell+1) - \phi(i,\ell), \quad \Delta_{-\tau} \phi(i,\ell) \equiv \phi(i,\ell) - \phi(i,\ell-1). \quad (1.86)$$

Note: It can be shown (Batrouni and Mabilat, 1999) that the world line representation is dual to the coherent state representation in the Kramers-Wannier sense (Kramers and Wannier, 1941).

1.3.2 Phase Diagram

Mapping the bosonic Hubbard model onto a $(D+1)$ classical model did not lead to a well known model whose phase diagram is already studied. However, one can form a good idea of its phase diagram by first looking at extreme cases. We recall first that this model has two independent control parameters, the density, ρ , and the interaction, U , or, in the grand canonical ensemble the chemical potential, μ , and the interaction, U . In what follows we shall examine the phase diagram in the $(t/U, \mu/U)$ plane (Fisher *et al.*, 1989).

One easy limiting case to study is the no-hopping limit, $t/U \rightarrow 0$. The Hamiltonian, in arbitrary dimensionality, reduces to the sum of single site Hamiltonians,

$$\mathcal{H} = \sum_{i=1}^N H_i \quad (1.87)$$

$$H_i = \frac{U}{2} \hat{n}_i (\hat{n}_i - 1) - \mu \hat{n}_i. \quad (1.88)$$

The ground state is obtained simply by minimizing H_i with respect to the site occupation for a fixed μ . It is easy to see (Fisher *et al.*, 1989) that for

$$(n-1) < \frac{\mu}{U} < n, \quad (1.89)$$

the site Hamiltonian, H_i , is minimized for a site occupation of n bosons/site. In other words,

$$0 < \frac{\mu}{U} < 1 \implies n = 1, \quad (1.90)$$

$$1 < \frac{\mu}{U} < 2 \implies n = 2, \quad (1.91)$$

$$2 < \frac{\mu}{U} < 3 \implies n = 3. \quad (1.92)$$

This means that as μ/U is increased from 0, the system will be stuck at one boson/site for the interval $0 < \frac{\mu}{U} < 1$ and as μ/U goes into the next interval, $1 < \frac{\mu}{U} < 2$, the occupation will change everywhere to two bosons/site and so on. This change in the density as μ/U is tuned at $T = 0$ is a quantum phase transition! Within each interval, the system is incompressible since the compressibility, $\kappa = \partial\rho/\partial\mu = 0$, it is also an insulator because there is no particle transport when $t/U = 0$. This incompressible insulating phase at multiples of full filling is called the Mott insulator.

We have, thus, established, that in the limit $t/U = 0$, the system passes through a series of Mott insulating phases. One can demonstrate via perturbation theory that as t/U increases (the interaction, U , decreases), the Mott regions shrink and eventually vanish. We demonstrate this here, to first order in t/U , by considering the n th Mott phase, $|M_n\rangle$. To take the system out of this phase, we can add one particle to it, creating a one-particle excitation $|P_n\rangle$, or remove a particle, creating a one-hole excitation $|H_n\rangle$. The properly normalized states are given by

$$\begin{aligned} |M_n\rangle &= |n, n, n, \dots, n\rangle, \quad (1.93) \\ &= \prod_{i=1}^N \frac{(a_i^\dagger)^n}{\sqrt{(n+1)!}} |0\rangle, \end{aligned}$$

$$|P_n\rangle = \frac{1}{\sqrt{N}} \sum_{i=1}^N \frac{a_i^\dagger}{\sqrt{n+1}} |M_n\rangle, \quad (1.94)$$

$$|H_n\rangle = \frac{1}{\sqrt{N}} \sum_{i=1}^N \frac{a_i}{\sqrt{n}} |M_n\rangle, \quad (1.95)$$

where $N = N_1 N_2 \dots N_D$. To first order in the perturbation, t/U , the energies of these states are simply given by the expectation values of \mathcal{H} . Since we are fixing the particle numbers here, the chemical potential, μ , should not be included in the Hamiltonian for this calculation. The energies are easy to obtain and are given by,

$$\begin{aligned} E(M_n) &= \langle M_n | \mathcal{H} | M_n \rangle, \\ &= \frac{U}{2} N n (n-1), \quad (1.96) \end{aligned}$$

$$\begin{aligned} E(P_n) &= \langle P_n | \mathcal{H} | P_n \rangle, \\ &= \frac{U}{2} N n (n-1) + U n - 2tD(n+1), \quad (1.97) \end{aligned}$$

$$\begin{aligned} E(H_n) &= \langle H_n | \mathcal{H} | H_n \rangle, \\ &= \frac{U}{2} N n (n-1) - U(n-1) - 2tDn \quad (1.98) \end{aligned}$$

Since $T = 0$ here, the internal energy is equal to the free energy which allows us to calculate the chemical potential for n particles as $\mu(n) = E(n) - E(n-1)$. The chemical potential where the $H_n - M_n$ transition takes place gives the lower boundary of the n th Mott region,

$$\frac{\mu_{lower}}{U} = \frac{1}{U} (E(M_n) - E(H_n)) = (n-1) + \frac{2Dt}{U}n, \quad (1.99)$$

while the upper boundary is given by the $P_n - M_n$ transition,

$$\frac{\mu_{upper}}{U} = \frac{1}{U} (E(P_n) - E(M_n)) = n - \frac{2Dt}{U}(n+1). \quad (1.100)$$

This gives the n th Mott gap, Δ_n ,

$$\Delta_n = \frac{\mu_{upper}}{U} - \frac{\mu_{lower}}{U} = 1 - \frac{2Dt}{U}(1+2n), \quad (1.101)$$

which vanishes at the critical coupling

$$\left(\frac{2Dt}{U}\right)_c = \frac{1}{2n+1}. \quad (1.102)$$

Equation (1.101) shows that in the $t/U \rightarrow 0$ limit the gap has unit width in agreement with Eq.(1.89) and that the effect of hopping is to make the Mott regions protrude into the finite t/U region while at the same time getting narrower. Equation (1.102) shows that these Mott regions eventually end at a critical value, $2Dt/U$, giving the Mott regions lobe-like shapes in the $(\mu/U, t/U)$ plane (see Fig. 1.4). See reference (Freericks and Monien, 1996) for a more elaborate treatment of perturbation to third order in t/U .

What is the phase of the system when the Mott insulator disappears? It is well known that a noninteracting bosonic system in two (three) dimensions undergoes Bose-Einstein condensation (BEC) at zero (finite) temperature. In the presence of weak interaction, this BEC is also known to become a superfluid (SF). In addition, at $T = 0$, the one dimensional system is superfluid but without BEC.

We therefore form (Fisher *et al.*, 1989) the following qualitative picture of the phase diagram: At small enough t/U , the system is in a Mott insulating phase when the density is an integer multiple of the number of sites. As t/U increases, the bosons can hop around the lattice more easily and the Mott insulators disappear to be replaced by a superfluid phase. The system is always superfluid when the number of particles is incommensurate with the number of sites. The phase diagram of the one-dimensional system, determined from Quantum Monte Carlo simulations, is shown in Fig. 1.4 clearly showing the Mott lobes. Going from the superfluid to the Mott phase, the system undergoes a quantum phase transition.

This qualitative picture will serve as the basis for a mean field calculation. But first, how does one determine if a phase is superfluid? Superfluidity is a quantum phenomenon where the phase of the wavefunction is coherent over macroscopic length scales. In such a case, the phase is said to be rigid or stiff: A twist in the phase at one

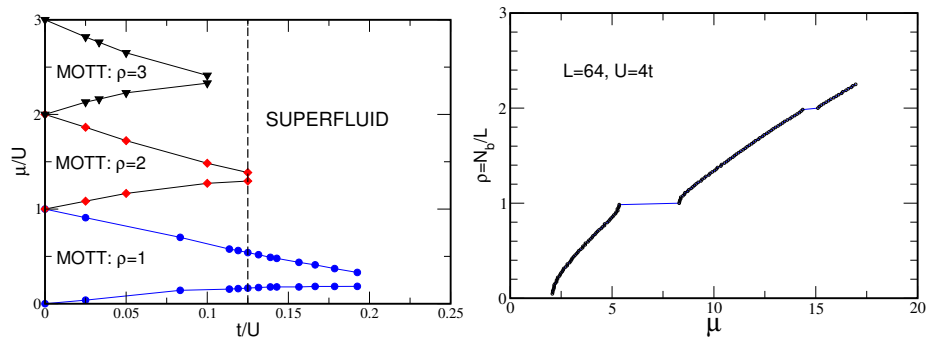


Fig. 1.4 Left: The ground state phase diagram of the one-dimensional bosonic Hubbard model, Eq.(1.65), from Quantum Monte Carlo simulations. The system is always superfluid for incommensurate filling. For commensurate filling, $\rho = 1, 2, 3, \dots$, the systems is a Mott insulator for strong coupling, small t/U , and superfluid for small coupling, large t/U . Right: A plot of ρ versus μ at fixed t/U along the dashed vertical in the left panel. In the horizontal plateaux $\kappa = \partial\rho/\partial\mu = 0$ indicating the incompressible Mott lobes. The transitions from the superfluid to the Mott insulator lobes are quantum phase transitions.

end of the system makes itself felt throughout. The average momentum in quantum mechanics is given by

$$\vec{p} = \langle \Psi | -i\hbar \vec{\nabla} | \Psi \rangle, \quad (1.103)$$

$$= \langle \Psi | \hbar \vec{\nabla} \phi(\vec{r}) | \Psi \rangle, \quad (1.104)$$

$$\equiv m \vec{v}_s, \quad (1.105)$$

where $\phi(\vec{r})$ is the phase of the wavefunction and \vec{v}_s is, by definition, the superfluid velocity. We see that $\vec{p} = 0$ if the phase of the wavefunction is not coherent. In other words, if the phase fluctuates with very short correlation length (called coherence length in this context), then the average of the gradient will vanish even over short length scales. If, on the other hand, the phase is coherent over long length scales, one can have $\vec{p} \neq 0$. One way, then, to probe for superfluidity, is to calculate the free energy of the system under normal periodic boundary conditions, $F(0)$, and then to measure the free energy with an externally imposed phase gradient, $\delta\phi$ (see below), $F(\delta\phi)$. The difference is nonzero only if the phase is rigid and is interpreted as the kinetic energy of the superfluid component due to the imposed velocity field (phase gradient) (Fisher *et al.*, 1973),

$$F(\delta\phi) = F(v_s) \approx F(0) + \rho_s \frac{Vm}{2} \vec{v}_s^2, \quad (1.106)$$

where V is the volume, m the mass of the bosons and ρ_s the number density of the superfluid component. Note that, since the wavefunction must be single valued, then in a system with periodic boundary conditions, *e.g.* superfluid helium in a toroidal container, the total phase change when the entire length of the system is traversed must be an integer multiple of 2π . Consequently,

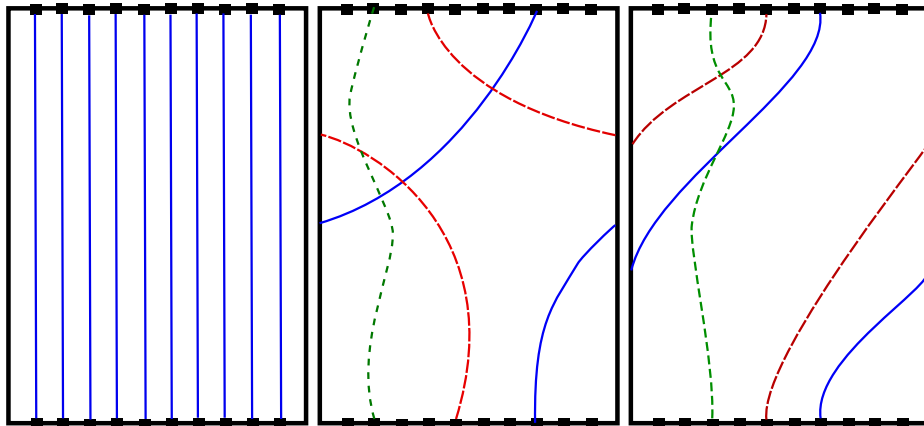


Fig. 1.5 Possible configurations of boson world lines. The horizontal axis is the space with the squares denoting lattice sites. The vertical axis is β , the imaginary time. Left panel shows a Mott insulator: The energy cost of double occupancy of a site is too high, the bosons occupation does not fluctuate and the bosons go straight along the imaginary time direction. Large quantum fluctuations are allowed for dilute systems or systems where the contact repulsion is not very large. The middle panel depicts such a case where the fluctuations are not coherent: The solid world line undergoes a large fluctuation giving it $W = 1$, the long dashed line gets $W = -1$ while the short dashed line has only small fluctuations. The total winding of this configuration is $W = 0$. The right panel shows a coherent fluctuation: The total winding is $W = 2$. A phase where, as a function of real time, the fluctuations tend to be like those of the center panel, the system is a normal (nonsuperfluid) quantum liquid. If the fluctuations are like those of the right panel, the system is in the superfluid phase.

$$\langle \vec{\nabla} \phi(\vec{r}) \rangle = \frac{m}{\hbar} \vec{v}_s = 2\pi n/L, \quad (1.107)$$

where L is the length of the system and n is an integer. The topological number n counts the number of times the phase winds as the system is traversed. This is the remarkable Onsager velocity quantization condition (Onsager, 1949) for superfluids and has been verified experimentally! Therefore, the superfluid density can be obtained from

$$\rho_s = \frac{1}{Vm} \frac{\partial^2 F(v_s)}{\partial v_s^2}. \quad (1.108)$$

In the world line representation discussed earlier, we can show that the superfluid density is given by (Pollock and Ceperley, 1987),

$$\rho_s = \frac{\langle W^2 \rangle}{tD\beta L^{D-2}} \quad (1.109)$$

where W , the “winding number”, is an integer giving the number of times the world lines wind around the lattice in the space direction. The configuration in Fig 1.2 has only $W = 0$. Equation (1.109) leads to an appealing physical picture for the phases of

the bosonic Hubbard model in terms of world lines. In Fig. 1.5 we show three possible configurations of world lines. The left panel shows the world line configuration with one boson/site and large U/t , in other words the Mott insulator. In this phase, the system is incompressible and the bosons cannot hop among the sites and therefore their world lines are straight lines in the imaginary time direction. The winding is strictly vanishing and $\rho_s = 0$. The center panel shows a normal (non-superfluid) bosonic quantum liquid. We choose a dilute system to keep the figure uncluttered. In this situation, there may be large enough quantum fluctuations to produce a world line with $W \neq 0$. However, the fluctuations are not coherent and, typically, there is an equal number of positive and negative windings at any given moment which keeps $W = 0$. However, note the differences between this situation and that of the Mott insulator. In the superfluid phase, the fluctuations are coherent and, typically, when a boson undergoes a large fluctuation it does this collectively with other particles leading to configurations such as the one depicted in the right panel of Fig. 1.2. When averaged over configurations, the situation depicted in the right panel will also give $\langle W \rangle = 0$ but it will have $\langle W^2 \rangle \neq 0$ whereas the situations depicted in the left and center panels will give $\langle W \rangle = \langle W^2 \rangle = 0$.

Scaling arguments (Fisher *et al.*, 1989) lead to the critical exponents $\nu = 1/2$ and $z = 2$ for all dimensions. These values lead to the prediction that as the system goes from the SF phase into a Mott lobe in Fig. 1.4, the superfluid density vanishes as $\rho_s \sim |\rho - \rho_c|$ where $\rho_c = 1$ for the first Mott lobe, $\rho_c = 2$ for the second etc. Figure 1.6 shows QMC results which confirm this prediction.

Note that, like the quantum Ising model discussed above, we have here $z\nu = 1$. However, in contradistinction with the quantum Ising model where the correlation length in the imaginary time direction diverged like the spatial correlation length, $\xi_\tau \sim \xi$ since $z = 1$ in that case, in the present case we have $\xi_\tau \sim \xi^2$: The space and imaginary time directions are not equivalent.

We now illustrate some of the critical properties of the bosonic Hubbard model using a simple but instructive method, namely mean field. We begin with a word of caution however. The mean field method is only as good as the guess for the mean field state and it is not reliable at low dimensions. Furthermore, this is not a controlled approximation in the sense that the error can be made arbitrarily small by including higher corrections. There are several ways, of varying sophistication, to implement a mean field calculation for the model Eq.(1.65) (Oosten *et al.*, 2001). Here we shall illustrate the simplest method applied to the hard core bosonic Hubbard model. In this model, the contact interaction between bosons is infinitely repulsive which, consequently, strictly forbids multiple occupation of a site. The Hamiltonian is given by

$$\mathcal{H} = -t \sum_{\langle i,j \rangle} (a_i^\dagger a_j + a_j^\dagger a_i) - \mu \sum_i \hat{n}_i, \quad (1.110)$$

with the condition that no multiple occupation is allowed. We now propose a mean field state,

$$|\Psi_{MF}\rangle = \prod_{i=1}^N (u + v a_i^\dagger) |\mathbf{0}\rangle, \quad (1.111)$$

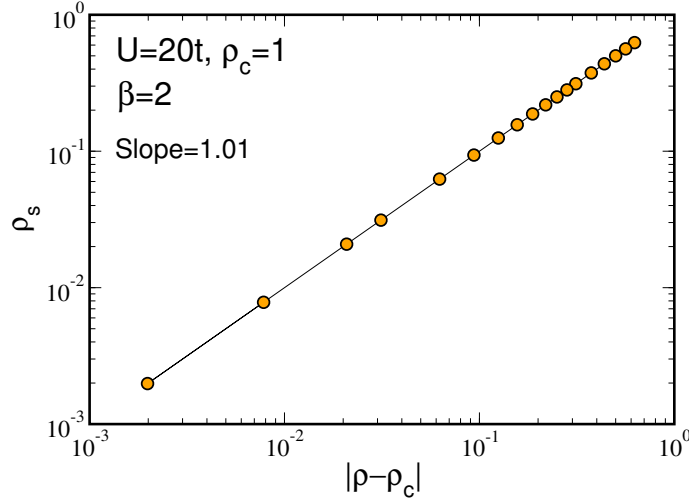


Fig. 1.6 The superfluid density, ρ_s , as a function of $|\rho - \rho_c|$, on log-log scale, for the one-dimensional bosonic Hubbard model. This confirms that $\rho_s \sim |\rho - \rho_c|$. Note that although $\beta = 2$ does not seem to be very large, the system is essentially in its ground state because the thermal energy, β^{-1} , is much smaller than U . The systems sizes used ranged from $N = 16$ to $N = 256$.

where $|\mathbf{0}\rangle$ is the empty state, $a_i|\mathbf{0}\rangle = 0$. In Eq.(1.111), u (v) is the amplitude that site i is vacant (occupied) and, consequently, we have $u^2 + v^2 = 1$ which ensures that $\langle \Psi_{MF} | \Psi_{MF} \rangle = 1$. This can be written as

$$u = \sin(\theta/2), \quad v = \cos(\theta/2), \quad (1.112)$$

The angle, θ , will be determined by minimizing the grand potential,

$$\Gamma = \langle \Psi_{MF} | \mathcal{H} | \Psi_{MF} \rangle. \quad (1.113)$$

Keeping in mind the hard core condition of no multiple occupancy ($a_i^\dagger a_i^\dagger |\mathbf{0}\rangle = 0$), it is easy to show that,

$$\begin{aligned} \Gamma &= -t \sum_{\langle i,j \rangle} \langle \mathbf{0} | (u + va_i)(u + va_j)(a_i^\dagger a_j + a_j^\dagger a_i)(u + va_i^\dagger)(u + va_j^\dagger) | \mathbf{0} \rangle \\ &\quad - \mu \sum_i \langle \mathbf{0} | (u + va_i) \hat{n}_i (u + va_i^\dagger) | \mathbf{0} \rangle, \end{aligned} \quad (1.114)$$

$$\begin{aligned} &= -2tDu^2v^2N - \mu v^2N, \\ &= -2tDN \sin^2(\theta/2) \cos^2(\theta/2) - \mu N \cos^2(\theta/2), \\ &= -\frac{tDN}{2} \sin^2(\theta) - \frac{\mu N}{2} (1 + \cos(\theta)) \end{aligned} \quad (1.115)$$

where D is the number of space dimensions and N is the number of sites. Minimizing Γ with respect to θ , $\partial\Gamma/\partial\theta = 0$, gives

$$\cos(\theta) = \frac{\mu}{2tD}, \quad (1.116)$$

and consequently,

$$\Gamma = -\frac{tDN}{2} \left(1 + \frac{\mu}{2tD}\right)^2. \quad (1.117)$$

The density as a function of the chemical potential is given by

$$\rho = -\frac{1}{N} \frac{\partial \Gamma}{\partial \mu} = \frac{1}{2} + \frac{\mu}{4tD}. \quad (1.118)$$

Note that from Eq.(1.116) we have the condition that $-1 \leq \mu/2tD \leq 1$ and, therefore, Eq.(1.118) gives $0 \leq \rho \leq 1$ as required by the hardcore condition.

The condensate, which is the order parameter, is given by the number of particles in the $k = 0$ quantum level,

$$N_0 = \langle \Psi_{MF} | \tilde{a}_0^\dagger \tilde{a}_0 | \Psi_{MF} \rangle, \quad (1.119)$$

where \tilde{a}_k is the Fourier transform of a_i ,

$$\tilde{a}_{\vec{k}} = \frac{1}{\sqrt{N}} \sum_{\vec{r}} a_{\vec{r}} e^{i\vec{k} \cdot \vec{r}}. \quad (1.120)$$

The periodic boundary conditions we took impose,

$$\vec{k} = \left(\frac{2\pi n_1}{N_1}, \frac{2\pi n_2}{N_2} \dots \frac{2\pi n_D}{N_D} \right), \quad (1.121)$$

where N_i is the number of sites along the i th direction, $-N_i/2 \leq n_i \leq N_i/2 - 1$, and $N = N_1 N_2 \dots N_D$. The condensate is, therefore, given by

$$\begin{aligned} N_0 &= \frac{1}{N} \sum_{i,j} \langle \Psi_{MF} | a_i^\dagger a_j | \Psi_{MF} \rangle, \\ &= \frac{1}{N} \sum_{i \neq j} \langle \mathbf{0} | (u + va_i)(u + va_j) a_i^\dagger a_j (u + va_i^\dagger)(u + va_j^\dagger) | \mathbf{0} \rangle \\ &\quad + \frac{1}{N} \sum_i \langle \mathbf{0} | (u + va_i) a_i^\dagger a_i (u + va_i^\dagger) | \mathbf{0} \rangle, \end{aligned} \quad (1.122)$$

$$= (N-1)u^2v^2 + v^2, \quad (1.123)$$

$$\approx \frac{N}{4} \left(1 - \left(\frac{\mu}{2tD} \right)^2 \right), \quad (1.124)$$

$$= N\rho(1-\rho), \quad (1.125)$$

where, going from Eq.(1.123) to Eq.(1.124) we kept only the term of order N and used Eq.(1.116). We see that as the Mott lobe, $\rho_c = 1$, is approached, the condensate fraction, $\rho_0 = N_0/N$, vanishes as a power with exponent equal to 1, $(\rho_c - \rho)$.

In addition to the order parameter, ρ_0 , we can calculate the superfluid density, ρ_s , by imposing an external phase gradient on the system (Bernardet *et al.*, 2002).

$$\mathcal{H}_{\delta\phi} = -t \sum_{\langle i,j \rangle} \left(a_i^\dagger e^{i\delta\phi} a_j + a_j^\dagger e^{-i\delta\phi} a_i \right) - \mu \sum_i \hat{n}_i, \quad (1.126)$$

where the constant phase gradient, $\delta\phi$, is nonzero along only one direction and vanishes along the other directions. Taking the expectation value of this Hamiltonian in the mean field state gives,

$$\Gamma_{\delta\phi} = -2t(D-1)Nu^2v^2 - 2tNu^2v^2 \cos(\delta\phi) - \mu Nv^2, \quad (1.127)$$

$$\approx -2tDNu^2v^2 + tNu^2v^2(\delta\phi)^2 - \mu Nv^2, \quad (1.128)$$

$$= \Gamma + tNu^2v^2(\delta\phi)^2, \quad (1.129)$$

$$= \Gamma + \frac{m}{2}Nu^2v_s^2. \quad (1.130)$$

To get the last equation we used Eq.(1.107) and the fact that the hopping parameter corresponds to $t = \hbar^2/2m$. The superfluid density is therefore given by,

$$\rho_s = \frac{1}{Nm} \frac{\partial^2 \Gamma_{\delta\phi}}{\partial v_s^2}, \quad (1.131)$$

$$= u^2v^2, \quad (1.132)$$

$$= \rho(1 - \rho). \quad (1.133)$$

We see that at this level of mean field approximation, the condensate fraction and the superfluid density are equal. Furthermore, ρ_s vanishes linearly with $(1 - \rho)$ as predicted by the scaling arguments mentioned above and from QMC. This mean field result is shown (dot-dash line) in Fig.1.7 up to $\rho = 1/2$; the curve is symmetric with respect to that point.

One can improve on this approximation by taking fluctuations into account (Bernardet *et al.*, 2002). Doing that lifts the degeneracy between ρ_0 and ρ_s . The result of this calculation (Bernardet *et al.*, 2002) in two dimensions is shown in Fig.1.7 and compared with exact QMC results. The very close agreement between the exact QMC results and the mean field plus fluctuations is quite remarkable. Such close quantitative agreement between mean field and exact results is rather unusual. Note, in addition, that $\rho_s > \rho_0$. This emphasizes the important fact that the condensate and the superfluid fraction should not be considered to be the same: They are not. Quantum fluctuations can knock bosons out of the the $k = 0$ level, reducing ρ_0 , and bosons in the higher momentum states can participate in superfluid transport, thus increasing ρ_s .

Similar close agreement is obtained in three dimensions. Not surprisingly, this calculation fails in one dimension. One aspect of this failure is that one finds, in $D = 1$, that the condensate fraction, ρ_0 , is still given by Eq.(1.125) whereas it is well known that $\rho_0 = 0$ in this case.

Practice problem: Hard core bosons are somewhat awkward to handle. They satisfy the commutation relations,

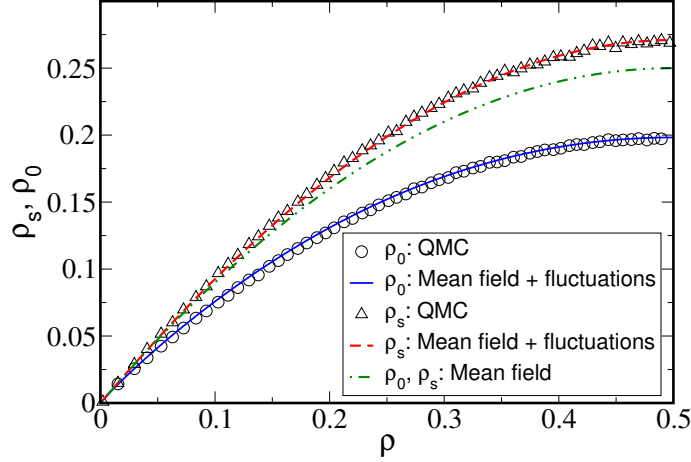


Fig. 1.7 The solid line shows the condensate fraction, ρ_0 , and the dashed line shows the superfluid density, ρ_s , for the $D = 2$ hardcore bosonic Hubbard model using the corrected mean field approximation (see text). The dot-dash line is the lowest order mean field result for both ρ_s and ρ_0 (Eq.(1.133)).

$$[a_i, a_j] = [a_i^\dagger, a_j^\dagger] = 0, \quad (1.134)$$

and for $i \neq j$,

$$[a_i, a_j^\dagger] = 0. \quad (1.135)$$

But since for hardcore bosons we have $a^\dagger|1\rangle = 0$, it is easy to show that, instead of the usual commutation relation $[a_i, a_i^\dagger] = 1$, we have

$$a_i a_i^\dagger + a_i^\dagger a_i = 1. \quad (1.136)$$

In fact, hard core bosons can be easily mapped to a spin-1/2 system via $a_i \rightarrow \sigma_i^-$, $a_i^\dagger \rightarrow \sigma_i^+$ and $a^\dagger a_i = n_i \rightarrow \sigma_i^z + 1/2$. This mapping is valid in any dimension (Bernardet *et al.*, 2002), but for $D = 1$ we can use in addition the Jordan-Wigner transformation (see the appendix) to diagonalize the resulting Hamiltonian Eq.(1.110). Show that

$$1 - 2c_j^\dagger c_j = e^{i\pi c_j^\dagger c_j}, \quad (1.137)$$

where c_i and c_i^\dagger are fermionic operators. Use the Jordan-Wigner transformation to express Eq.(1.126) as

$$\mathcal{H}_{\delta\phi} = -t \sum_{i=1}^N \left(c_i^\dagger e^{i\delta\phi} c_{i+1} + c_{i+1}^\dagger e^{-i\delta\phi} c_i \right) - \mu \sum_{i=1}^N c_i^\dagger c_i. \quad (1.138)$$

By using Fourier transformation, show that

$$\mathcal{H}_{\delta\phi} = \sum_{k=1}^N \epsilon_k c_k^\dagger c_k, \quad (1.139)$$

$$\epsilon_k = -2t \cos(\delta\phi + k) - \mu. \quad (1.140)$$

In the ground state (*i.e.* at zero temperature) there is one fermion per value of k and terminates at N_b , the number of original bosons present,

$$\mathcal{H}_{\delta\phi} = \sum_{k=1}^{N_b} \epsilon_k. \quad (1.141)$$

Show that the superfluid density is given by

$$\rho_s = \frac{1}{N} \sum_{n=1}^{N_b} \cos\left(\frac{2\pi}{N}n\right), \quad (1.142)$$

and perform the sum. Show that $\rho_s = 0$ for $\rho = N_b/N = 1$ and that for very dilute systems $\rho_s = \rho$.

Practice problem: In this problem we will perform a rudimentary mean field calculation for soft core bosonic Hubbard model, Eq.(1.65), which has the virtue of simplicity and ease of calculation and which will give a qualitative picture of the phase diagram. On the other hand, due to its simplicity, it will not be very accurate quantitatively. This calculation is based on a straight forward generalization of the method used for hard core bosons where we took the mean field state,

$$|\Psi_{MF}\rangle = \prod_{i=1}^N (u + v a_i^\dagger) |\mathbf{0}\rangle, \quad (1.143)$$

with the condition $a_i^\dagger a_i^\dagger |\mathbf{0}\rangle = 0$. In this case, the calculation described the system for $0 \leq \rho \leq 1$. Now we propose the mean field state

$$|\Psi_{MF}^n\rangle = \prod_{i=1}^N \left(u + \frac{v}{\sqrt{n+1}} a_i^\dagger\right) |\mathbf{n}\rangle, \quad (1.144)$$

where the state $|\mathbf{n}\rangle$ has n bosons/site. In analogy with the hard core case, u is the amplitude to have n particles on a site, and v is the amplitude to create a particle and have $(n+1)$ particles on that site; $u^2 + v^2 = 1$. Furthermore, we impose the condition $a_i^\dagger a_i^\dagger |\mathbf{n}\rangle = 0$: We cannot create two particles on top of the n particles already present, only one creation is allowed. Consequently, $|\Psi_{MF}^n\rangle$ can only describe the system for $n \leq \rho \leq n+1$. It is clear that this mean field state is a poor choice when t/U is large because at weak coupling large fluctuations are not uncommon.

Show that,

$$\frac{\Gamma_n}{N} = \frac{\langle \Psi_{MF}^n | \mathcal{H} | \Psi_{MF}^n \rangle}{N} = -2tDu^2v^2(n+1) + u^2 \left[\frac{U}{2}n(n-1) - \mu n \right] + v^2 \left[\frac{U}{2}n(n+1) - \mu(n+1) \right]. \quad (1.145)$$

Writing $u = \sin(\theta/2)$ and $v = \cos(\theta/2)$, minimize Γ_n with respect to θ and show that

$$\cos(\theta) = \frac{\mu - Un}{2tD(n+1)}. \quad (1.146)$$

Substituting in Eq.(1.145), show that

$$\frac{\Gamma_n}{N} = -\frac{t}{2}D(n+1) \left[1 + \frac{\mu - Un}{2tD(n+1)} \right]^2 + \frac{1}{2} [Un^2 - Un - 2\mu n]. \quad (1.147)$$

Calculate

$$\rho^n = -\frac{1}{N} \frac{\partial \Gamma_n}{\partial \mu}, \quad (1.148)$$

and show that $n \leq \rho^n \leq n+1$. Hint: Look at Eq.(1.146).

Now we want to calculate the boundaries of the Mott lobes. Since $n \leq \rho^n \leq n+1$, the lower boundary, μ_n^-/U , of the n th Mott lobe comes from $\rho_{\max}^{(n+1)} = n$ and the upper boundary, μ_n^+/U , comes from $\rho_{\min}^n = n$. Show that

$$\frac{\mu_n^-}{U} = (n-1) + 2Dn \frac{t}{U}, \quad (1.149)$$

$$\frac{\mu_n^+}{U} = n - 2D(n+1) \frac{t}{U}. \quad (1.150)$$

Draw the phase diagram in the $(t/U, \mu/U)$ plane and compare with Fig. 1.4. The Mott gap, the width of the Mott lobe at t/U , can be calculated from $(\mu_n^+ - \mu_n^-)/U$. Show that the n th lobe terminates at the critical value

$$\frac{t}{U_c} = \frac{1}{2D(2n+1)}. \quad (1.151)$$

This shows that the tip of the n th lobe recedes as n^{-1} for large n and agrees with more elaborate mean field calculations. following the calculation in the hard core case, show that the condensate fraction is given by,

$$\rho_0 = (n+1)(\rho - n)(1 + n - \rho). \quad (1.152)$$

This expression holds between two Mott lobes, the n th and $(n+1)$ th. So, the critical densities are $\rho_c = n$ and $\rho_c = (n+1)$ and we, therefore, see that the condensate vanishes as $\rho_0 \sim |\rho - \rho_c|$. The superfluid density can be calculated by imposing a gradient, as before. Show that ρ_s is given by Eq.(1.152).

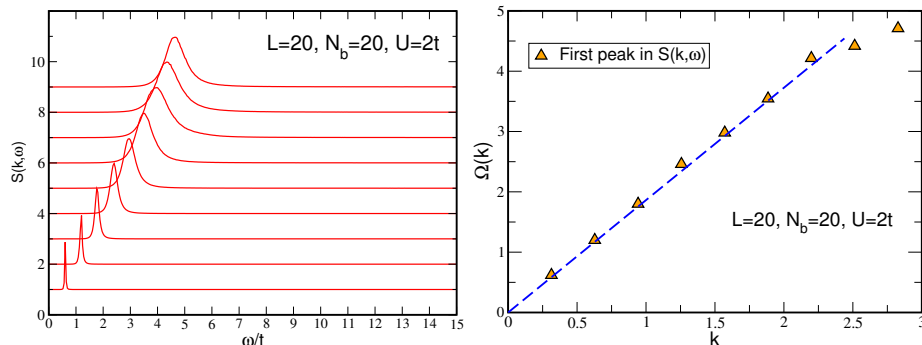


Fig. 1.8 The superfluid phase. Left: $S(k, \omega)$ for the bosonic Hubbard model in $D = 1$ obtained by using the maximum entropy method to obtain the Laplace transform with respect to τ of $S(k, \tau)$. The horizontal axis is the frequency (*i.e.* energy), each curve corresponds to a different k value. The lowest curve is $k = 2\pi/L$ and moves up to $k = 2\pi(L/2 - 1)/L \approx \pi$. Right: The dispersion relation of excitations is obtained from the positions of the peaks of $S(k, \omega)$ as a function of k . We see that the dispersion in the superfluid phase is linear for small k . The linear dispersion indicates phonon excitations and a stable superfluid phase.

Note that due to the constraint that only one particle can be created this approximation gives nonsensical results beyond the tips of the Mott lobes. Also note that Eqs.(1.149-1.151) agree with the perturbation results Eqs.(1.99-1.102). This is because we used the same states in both cases and because in both cases the energies are just the expectation values of the Hamiltonian. In the perturbation case we fixed the particle number and then calculated the chemical potential; in the mean field case, we fixed the chemical potential which we used as a variational parameter. Higher order perturbations and more elaborate mean field do not give identical results.

1.3.3 Dynamics

The mapping of D -dimensional quantum systems onto $(D + 1)$ -dimensional classical systems has yielded insights into the behavior of both classical and quantum systems. One property of quantum systems not shared by classical ones is their dynamics: Once the Hamiltonian is written, the dynamics of the quantum system are determined. As discussed above in section 1.1.2, the additional dimension introduced because of the mapping onto a classical model can be interpreted as the (imaginary) time axis and can, thus, be exploited to study dynamic effects. For example, excitation spectra can be obtained by performing a numerical Laplace transform on Eq.(1.20) using the Maximum Entropy method (Gubernatis *et al.*, 1991).

We now discuss briefly the properties of the dynamic density-density correlation function of the bosonic Hubbard model (in $D = 1$) and what it tells us about the excitation spectrum and transport properties. The dynamic density-density correlation function is obtained by taking $\tilde{\mathcal{O}}(\vec{k}, 0) = \tilde{n}(\vec{k}, 0)$ in Eq.(1.20).

We will consider a 1-dimensional lattice with $L = 20$ sites on which we place $N_b = 20$ bosons. We are interested in the ground state properties of the system and to

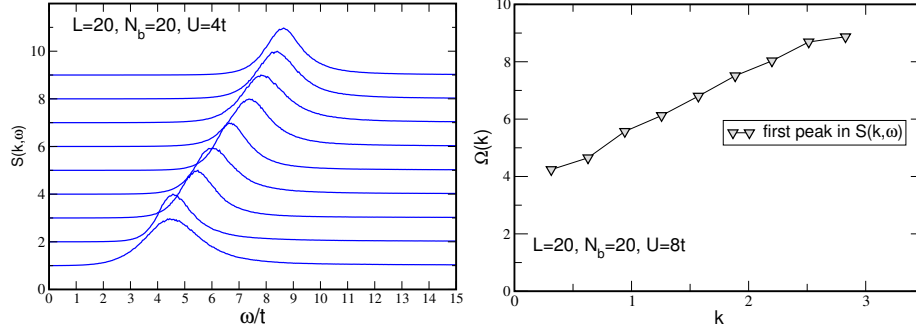


Fig. 1.9 The Mott insulating phase. Left: $S(k, \omega)$ from the maximum entropy method. Note that the peaks are wider. In fact, exact diagonalization of small systems reveals that each wide bump is composed of several peaks which maximum entropy merges into one. In addition, as $k \rightarrow 0$, the excitation energy does not go to zero: It takes a finite energy to produce excitations. This is the Mott gap and is seen clearly in the right panel where $\Omega(k=0) \approx 4t$. Figure 1.4 gives a value of $3t$ for this value of U . The uncertainty is due to the width of the peaks in the right panel.

that end we take $\beta = 20t$ which corresponds to a low enough temperature. We study two cases, $U = 2t$ which, according to Fig. 1.4, is in the superfluid phase and $U = 8t$ which is in the first Mott insulator lobe.

The left panel of Fig. 1.8 shows $S(k, \omega)$ for $\pi/10 \leq k \leq 9\pi/10$ obtained from the Laplace transform of $S(k, \tau)$ when $U = 2t$. For each k value, we see a peak corresponding to the excitation energy at that momentum. As k increases, the peaks get wider but remain relatively narrow. In fact, exact diagonalization of smaller systems (Roth and Burnett, 2004) shows that the wider peaks consist of several narrow peaks bunched close together which Maximum entropy cannot resolve. Plotting the location of each peak, *i.e.* energy, versus the momentum, k , yields the dispersion relation of the excitations and is shown in the right panel of Fig. 1.8. We see that the dispersion is linear for the smaller values of k indicating that the excitations are phonons and the superfluid is stable. Note that as $k \rightarrow 0$, the excitation energy $\Omega(k) \rightarrow 0$.

The behavior is different when $U = 8t$ and the system is in the Mott insulating phase. The left panel in Fig. 1.9 shows $S(k, \omega)$ which exhibits distinct features not present for $U = 2t$. For example, all the peaks are rather wide indicating that each is a collection of peaks representing a pack of closely spaced excited states. This means that the precise location of the lowest excitation energy is not easy to determine. In the right panel is shown the location of the peak maximum versus the momentum. It is clear that as $k \rightarrow 0$, $\Omega(k \rightarrow 0)$ is nonvanishing: There is an energy gap to produce the lowest excited state. This is one of the characteristics of the Mott insulator. However, note that while the energy gap calculated here is $\Omega(k \rightarrow 0) \approx 4t$, the value obtained from ρ versus μ in fig. 1.4 (right panel) is $3t$. The discrepancy is easy to understand: The gap in fig. 1.4 is the energy needed to reach the first excited state whereas the value obtained from fig. 1.9 corresponds to a higher excited state in the middle of a group of excited states. However, note that, for the smallest k value, the value of ω/t

where $S(k, \omega)$ rises appreciably does correspond to a value $\omega/t \approx 3t$.

The above example illustrates the utility of the formal interpretation of the β direction as imaginary time and how it can be exploited to obtain information not easily accessible otherwise. Here we only showed particle excitations obtained from the dynamic density-density correlation function. Other excitations can be calculated by using different operators for \mathcal{O} ; for example $\langle 0|a(\vec{r}', \tau)a^\dagger(\vec{r}, 0)|0\rangle$ yields the density of states.

1.4 Conclusions

We have presented in these lectures a pedagogical introduction to quantum phase transitions and some of the ideas and methods used to study this fascinating and very active subject. The experimental realization of trapped ultra-cold boson and fermion atomic systems loaded on optical lattices, provides actual systems governed by the type of Hamiltonians we studied here. These systems are very versatile because the Hamiltonian parameters are tunable and thus allow the experimental exploration of the many exotic phases and phases transitions expected in these models.

1.5 Appendix: The Jordan-Wigner Transformation

The Jordan-Wigner transformation is not within the scope of these lectures but I will simply present it in this appendix because it is useful and interesting and to point out why it does not work in more than one dimension.

Consider the following relations,

$$\sigma_i^z = 1 - 2c_i^\dagger c_i, \quad (1.153)$$

$$\sigma_i^+ = \prod_{j<i} (1 - 2c_j^\dagger c_j) c_i, \quad (1.154)$$

$$\sigma_i^- = \prod_{j<i} (1 - 2c_j^\dagger c_j) c_i^\dagger, \quad (1.155)$$

where $\sigma^\pm = (\sigma^x \pm i\sigma^y)$ are raising (+) and lowering (−) operators for z component of the spin. c_i and c_i^\dagger are operators whose commutation relations are determined from those of the the Pauli matrices,

$$[\sigma_i^+, \sigma_j^-] = \delta_{i,j} \sigma_i^z, \quad [\sigma_i^z, \sigma_j^\pm] = \pm \delta_{i,j} \sigma_i^\pm. \quad (1.156)$$

Inverting Eqs.(1.154-1.155) gives

$$\begin{aligned} c_i &= \left(\prod_{j<i} \sigma_j^z \right) \sigma_i^+ \\ c_i^\dagger &= \left(\prod_{j<i} \sigma_j^z \right) \sigma_i^-, \end{aligned} \quad (1.157)$$

with which it can be verified easily that

$$\{c_i, c_j^\dagger\} = \delta_{i,j}, \quad \{c_i, c_j\} = \{c_i^\dagger, c_j^\dagger\} = 0. \quad (1.158)$$

Therefore c_i and c_i^\dagger are *fermionic* annihilation and creation operators. Notice that central to this transformation is the product for $j < i$ of σ_j^z in Eq.(1.157) which, in effect, gives the operators σ_i^\pm tails extending all the way to the edge of the system. In one dimension, there is only one way to lay this tail and the transformation works. But in higher dimensions, the path taken by the tail is not unique: There is an infinity of tails (in the thermodynamic limit) and the Jordan-Wigner transformation fails for $D > 1$ (see below).

The above transformation is the conventional Jordan-Wigner transformation, but for the Hamiltonian Eq.(1.28), it is more convenient to rotate the spin axis,

$$\sigma^z \rightarrow \sigma^x, \quad \sigma^x \rightarrow -\sigma^z. \quad (1.159)$$

Equations (1.154-1.155) then become,

$$\sigma_i^x = 1 - 2c_i^\dagger c_i, \quad (1.160)$$

$$\frac{1}{2}(-\sigma_i^z + i\sigma_i^y) = \prod_{j<i} (1 - 2c_j^\dagger c_j) c_i, \quad (1.161)$$

$$\frac{1}{2}(-\sigma_i^z - i\sigma_i^y) = \prod_{j<i} (1 - 2c_j^\dagger c_j) c_i^\dagger, \quad (1.162)$$

and therefore

$$\sigma_i^z = -\prod_{j<i} (1 - 2c_j^\dagger c_j) (c_i^\dagger + c_i). \quad (1.163)$$

We then have,

$$\begin{aligned} \sigma_{i+1}^z \sigma_i^z &= \prod_{k<i+1} (1 - 2c_k^\dagger c_k) (c_{i+1} + c_{i+1}^\dagger) \prod_{j<i} (1 - 2c_j^\dagger c_j) (c_i + c_i^\dagger), \\ &= \prod_{k<i} (1 - 2c_k^\dagger c_k) (1 - 2c_i^\dagger c_i) (c_{i+1} + c_{i+1}^\dagger) \prod_{j<i} (1 - 2c_j^\dagger c_j) (c_i + c_i^\dagger), \\ &= \left(\prod_{k<i} (1 - 2c_k^\dagger c_k) \right)^2 (1 - 2c_i^\dagger c_i) (c_{i+1} + c_{i+1}^\dagger) (c_i + c_i^\dagger), \\ &= (1 - 2c_i^\dagger c_i) (c_{i+1} + c_{i+1}^\dagger) (c_i + c_i^\dagger), \\ &= c_{i+1} c_i + c_i^\dagger c_{i+1}^\dagger + c_{i+1}^\dagger c_i + c_i^\dagger c_{i+1}. \end{aligned} \quad (1.164)$$

Notice how the tails in the Jordan-Wigner transformation disappeared: The overlap of the tails gave the square of a term whose value is ± 1 . For this transformation to work, it is crucial that the tails overlap this way. That is why this fails in higher dimensions, there infinitely many ways to thread the tail through the system without overlap. With Eq.(1.164), the Hamiltonian, Eq.(1.28) becomes

$$\mathcal{H} = -J \sum_{i=1}^N \left(c_i^\dagger c_{i+1} + c_{i+1}^\dagger c_i + c_i^\dagger c_{i+1}^\dagger + c_{i+1} c_i + 2g c_i^\dagger c_i - g \right), \quad (1.165)$$

where we put $h = gJ$. To diagonalize Eq.(1.165), we first apply the Fourier transformation,

$$c_k = \frac{1}{\sqrt{N}} \sum_{\ell=1}^N c_\ell e^{-ik\ell}, \quad (1.166)$$

which gives,

$$\mathcal{H} = J \sum_k \left(2[g - \cos(ka)]c_k^\dagger c_k - i \sin(ka)[c_{-k}^\dagger c_k^\dagger + c_{-k} c_k] \right), \quad (1.167)$$

where $k = 2\pi n/N$, $n = -N/2, -(N-1)/2, \dots, 0, 1, 2, \dots, (N-1)/2$ and a is the lattice constant which we will take to be unity. Now we apply the Bogoliubov transformation,

$$\gamma_k = u_k c_k - i v_k c_{-k}^\dagger, \quad (1.168)$$

$$c_k = u_k \gamma_k + i v_k \gamma_{-k}^\dagger, \quad (1.169)$$

where γ_k is a new fermionic operator. In order for γ_k and γ_k^\dagger to satisfy the usual fermionic anticommutation relations, Eq.(1.158), one can show that u_k and v_k are real functions subject to the conditions $u_{-k} = u_k$, $v_{-k} = v_k$ and $u_k^2 + v_k^2 = 1$. This last condition can be expressed as $u_k = \sin(\theta_k)$, $v_k = \cos(\theta_k)$. Substituting Eq.(1.169) in Eq.(1.167) and requiring that the resulting Hamiltonian only contain terms of the form $\gamma_k^\dagger \gamma_k$ fixes the angle θ_k ,

$$\tan\theta_k = \frac{\sin(k)}{\cos(k) - g}, \quad (1.170)$$

and gives for the diagonalized Hamiltonian,

$$\mathcal{H} = \sum_k \epsilon_k \left(\gamma_k^\dagger \gamma_k - \frac{1}{2} \right), \quad (1.171)$$

$$\epsilon_k = 2J (1 + g^2 - 2g \cos(k))^{1/2}. \quad (1.172)$$

As mentioned above, the Jordan-Wigner transformation is very useful in $D = 1$ but fails in higher dimensions due to the certainty of non-overlapping tails.

References

- Batrouni, G. G. and Mabilat, H. (1999). *Comp. Phys. Comm.*, **121-122**, 468.
- Batrouni, G. G. and Scalettar, R. T. (1992). *Phys. Rev.*, **B46**, 9051.
- Batrouni, G. G. and Scalettar, R. T. (2000). *Phys. Rev. Lett.*, **84**, 1599.
- Baxter, R. J. (1982). *Exactly Solved Models in Statistical Mechanics*. Academic Press, New York.
- Bernardet, K., Batrouni, G. G., Meunier, J.-L., Schmid, G., Troyer, M., and Dorneich, A. (2002). *Phys. Rev.*, **B65**, 104519.
- Fazekas, P. (1999). *Lecture Notes on Electron Correlation and Magnetism*. World Scientific, Singapore.
- Fisher, M. E., Barber, M. N., and Jasnow, D. (1973). *Phys. Rev.*, **A8**, 1111.
- Fisher, M. P. A., Weichman, P. B., Grinstein, G., and Fisher, D. S. (1989). *Phys. Rev.*, **B40**, 546.
- Freericks, J.K. and Monien, H. (1996). *Phys. Rev.*, **B53**, 2691.
- Frey, E, Nelson, D. R., and Fisher, D. S. (1994). *Phys. Rev.*, **B49**, 9723.
- Gardiner, C. (2009). *Stochastic Methods: A Handbook for the Natural and Social Sciences*. Springer, Berlin.
- Gubernatis, J. E., Jarrell, Mark, Silver, R. N., and Sivia, D. S. (1991). *Phys. Rev.*, **B44**, 6011.
- Gutzwiller, M.C. (1963). *Phys. Rev. Lett.*, **10**, 159.
- Hirsch, J. E., Sugar, R. L., Scalapino, D. J., and Blankenbecler, R. (1992). *Phys. Rev.*, **B46**, 9051.
- Hohenberg, P. C. and Halperin, B. I. (1989). *Rev. Mod. Phys.*, **B40**, 546.
- Hubbard, J. (1964). *Proc. Roy. Soc.*, **A276**, 238.
- Jaksch, D., Bruder, C., Cirac, J.I., Gardiner, C.W., and Zoller, P. (1998). *Phys. Rev. Lett.*, **81**, 3108.
- Kanamori, J. (1963). *Prog. Theor. Phys.*, **30**, 275.
- Kramers, H. A. and Wannier, G. H. (1941). *Phys. Rev.*, **60**, 252.
- LeBellac, M., Mortessagne, F., and Batrouni, G. G. (2004). *Equilibrium and Non-Equilibrium Statistical Thermodynamics*. Cambridge University Press, Cambridge.
- Ma, S.-K. (1985). *Statistical Mechanics*. World Scientific, Singapore.
- Negele, J. W. and Orland, H. (1998). *Quantum Many-particle Systems*. Westview Press, Boulder.
- Niyaz, P., Scalettar, R. T., Fong, C.Y., and Batrouni, G. G. (1991). *Phys. Rev.*, **B44**, 7143.
- Niyaz, P., Scalettar, R. T., Fong, C.Y., and Batrouni, G. G. (1994). *Phys. Rev.*, **B50**, 362.
- Onsager, L. (1944). *Phys. Rev.*, **65**, 117.
- Onsager, L. (1949). *Nuovo Cimento*, **6**, 249.

- Oosten, D. Van, van der Straten, P., and Stoof, H. T. C. (2001). *Phys. Rev.*, **A63**, 053601.
- Pollock, E. L. and Ceperley, D. M. (1987). *Phys. Rev.*, **B36**, 8343.
- Prokof'ev, N. V., Svistunov, B. V., and Tupitsyn, I. S. (1998). *Phys. Lett.*, **A238**, 253.
- Rasetti, M. (1991). *The Hubbard Model- Recent Results*. World Scientific, Singapore.
- Roth, R. and Burnett, K. (2004). *J. Phys. B*, **37**, 3893.
- Sachdev, S. (1999). *Quantum Phase Transitions*. Cambridge University Press, Cambridge.
- Savit, R. (1980). *Rev. Mod. Phys.*, **52**, 453.
- Sondhi, S. L., Girvin, S. M., Carini, J. P., and Shahar, D. (1997). *Rev. Mod. Phys.*, **69**, 315.
- Stanley, H. E. (1971). *Introduction to Phase Transitions and Critical Phenomena*. Oxford University Press, Oxford.
- Tobochnik, J., Batrouni, G. G., and Gould, H. (1992). *Computers in Physics*, **6**, 673.